Microbial Dysbiosis Associated with Impaired Intestinal Na^+/H^+ Exchange Accelerates and Exacerbates Colitis in Ex-Germ Free Mice

Christy A. Harrison[1,2], Daniel Laubitz[1], Christina L. Ohland[3], Monica T. Midura-Kiela[1], Karuna Patil[3], David G. Besselsen[3], Deepa R. Jamwal[1], Christian Jobin[4]*, Fayez K. Ghishan[1]*, Pawel R. Kiela[1,2]*

[1]Department of Pediatrics, Steele Children's Research Center, Tucson Arizona, United States of America; *[2]Department of Immunobiology, University of Arizona College of Medicine, Tucson, Arizona, United States of America; [3]University Animal Care, University of Arizona, Tucson, Arizona, United States of America; [4]Department of Medicine, Division of Gastroenterology, University of Florida College of Medicine, Gainesville, Florida, United States of America*

* Shared senior authorship

Correspondence: Pawel R. Kiela, DVM, PhD, *University of Arizona, Steele Children's Research Center,* 1501 N. Campbell Ave, Rm. 6351, Tucson, AZ 85724. Fax: (520) 626-4141; Ph: (520) 626-9687; email: pkiela@peds.arizona.edu

Disclosures: All authors declare that there is no conflict of interest to disclose

Running Head: Colitogenic microbiome of $NHE3^{-/-}$ mice

Abstract

Intestinal epithelial Na^+/H^+ exchange facilitated by the apical NHE3 (*Slc9a3*) is a highly-regulated process inhibited by intestinal pathogens and in inflammatory bowel diseases. $NHE3^{-/-}$ mice develop spontaneous, bacterially-mediated colitis, and IBD-like dysbiosis. Disruption of epithelial Na^+/H^+ exchange in IBD may thus represent a host response contributing to the altered gut microbial ecology, and may play a pivotal role in modulating the severity of inflammation in a microbiome-dependent manner. To test whether microbiome fostered in an NHE3-deficient environment is able to drive mucosal immune responses affecting the onset or severity of colitis, we performed a series of cohousing experiments and fecal microbiome transplants into germ-free Rag-deficient or $IL\text{-}10^{-/-}$ mice. We determined that in the settings where the microbiome of NHE3-deficient mice was stably engrafted in the recipient host, it was able accelerate the onset and amplify severity of experimental colitis. NHE3-deficiency was characterized by the reduction in pH-sensitive butyrate-producing *Firmicutes* families *Lachnospiraceae* and *Ruminococcaceae* (Clostridia clusters IV and XIVa), with an expansion of inflammation-associated *Bacteroidaceae*. We conclude that the microbiome fostered by impaired epithelial Na^+/H^+ exchange enhances the onset and severity of colitis through disruption of the gut microbial ecology.

INTRODUCTION

The intestinal epithelium is the first innate barrier that protects from luminal commensal and pathogenic microbiota, and actively contributes to the development and function of the mucosal immune system. Several genetic IBD susceptibility loci have been linked to genes with critical roles in the epithelial cell function, and functional dynamic changes in tight junction maintenance, mucus and antimicrobial peptide secretion, endoplasmic reticulum (ER) stress, and insufficient autophagy.[1] One of the primary roles of epithelial cells, nutrient transport, has been known to be affected by the inflammatory process. Changes in membrane transport have been considered responsible for secondary symptoms such as nutritional deficiencies or inflammation-associated diarrhea, and not as primary contributors to the disease process. This view is gradually changing as we begin to understand the consequences of altered epithelial transport to the mucosal and systemic homeostasis, gut microbiome, and to the local inflammatory process itself.[2]

Apical Na^+/H^+ exchange at the brush border of the absorptive gut epithelia serves several purposes, all critical to maintaining mucosal homeostasis. It is the key contributor to transepithelial Na^+ and water absorption, provides acidic milieu at the brush border to support nutrient transport by providing an inwardly directed proton gradient utilized for short-chain fatty acid (SCFA) absorption, supports low pH needed to maintain a compact and impenetrable inner mucus layer, couples functionally with glucose and bicarbonate transport, and regulates intracellular pH.[3, 4] NHE3, the product of the *Slc9a3* gene, is considered to be the dominant isoform of the three apically expressed Na^+/H^+ exchangers (NHE2, 3, and 8).[5] Pro-inflammatory cytokines such as interferon gamma (IFNγ) and

tumor necrosis factor alpha (TNFα) reduce NHE3 expression and activity[6-8], a phenomenon also prominently observed *in vivo* in several models of experimental colitis[9-11], and in IBD patients.[11-14] NHE3 is also inhibited by bacterial toxins produced by *Vibrio cholerae*[15] or *Clostridium difficile*[16], and by enteropathogenic *E. coli* via a mechanism depending on the type III secretion system and EspF.[17] Since gel-forming mucins produced by goblet and epithelial cells require acidic pH to maintain their compacted concatenated ring structures[18], disruption of NHE3 and the ensuing elevated pH of the inner mucus layer is likely responsible for the observed increased penetration and eventually bacterial translocation to the lamina propria,[19] and stimulation of local immune response. Indeed, NHE3-deficient mice develop spontaneous colitis with features characteristic of human IBD.[20] Their resting mucosal IFNγ production is elevated with increased numbers of CD8α^+ T cells and NK cells as the main source of the cytokine in the intraepithelial and lamina propria compartments, and are dramatically susceptible to DSS-induced mucosal injury.[21] Spontaneous colitis could be completely ameliorated and the response to DSS delayed by the administration of broad-spectrum antibiotics,[20, 21] collectively providing strong evidence for the necessary role for the gut microbiome in the development of disease in this model. Moreover, NHE3-deficient mice develop a dramatic dysbiosis, reminiscent in some ways of the changes described among IBD patients.[22] These observations in the colon were further strengthened by an independent report by Engevik et al.[23] who reported ileal expansion of *Bacteroides thetaiotaomicron* in NHE3$^{-/-}$ mice, a verified colitogenic pathobiont.[24, 25] NHE3-status was the defining and dominant factor in driving dysbiosis in adoptively transferred NHE3/Rag2 double-knockout mice, a model characterized by dramatically accelerated and exacerbated progression of colitis.[26]

Current dogma holds that the immune system develops an aberrant and progressive overreaction to commensal microbes, leading to host-damaging autoimmune disease. However, until recently it was unclear whether the microbiome in IBD is causative or merely reflective of disease. Limited published data support the notion that a dysbiotic microbiome can either transfer susceptibility[27] or outright transmit colitis.[28] In this report, we hypothesized that loss of NHE3 mediates the onset of colitis by shaping the microbiota. Thus, we sought to determine if the dysbiotic microbiota developed from NHE3 deficiency is sufficient alone to transmit susceptibility to experimental colitis in an NHE3-sufficient host. We tested this via cohousing under specific-pathogen free (SPF) conditions, fecal microbiome transplant (FMT) into germ-free (GF) $Rag1^{-/-}$ mice followed by adoptive T cell transfer, and FMT into GF $IL10^{-/-}$ mice. Dysbiosis was stably maintained only in $IL10^{-/-}$ FMT recipients, a model known for the inhibition of the endogenous NHE3.[10] In this host, significant reductions of butyrate-producing *Firmicutes* families *Lachnospiraceae* and *Ruminococcaceae* and an expansion of *Bacteroidaceae* correlated with earlier onset and increased colitis severity. These observations provide evidence that disruption of the intestinal Na^+/H^+ exchange during inflammation results in a microbial environment fostering mucosal inflammatory responses.

RESULTS

Dysbiotic microbiome or susceptibility to T cell-mediated colitis are not transferred from NHE3$^{-/-}$ to wild-type (WT) mice via passive microbiome sharing

Microbiome is a vital part of the pathogenesis of colitis associated with the loss of NHE3. Cohousing was chosen as the first approach to address the question whether microbial dysbiosis precipitated by NHE3 deficiency is dominant, passively transferrable, and sufficient to transmit susceptibility to experimental T cell-mediated colitis. All mice were raised and maintained in an ultraclean barrier facility (see description in the Methods section). Rag2$^{-/-}$ (Rag) mice were co-housed with either NHE3xRag2$^{-/-}$ double knockout (DKO) mice in a ratio of 2:3 Rag:DKO, or with other Rag mice as a control (Fig. S1A). As coprophagic animals, mice continually share their microbiome by consuming their own and their cage-mates' fecal pellets.[29] Cohousing has been demonstrated in several studies as efficient means of horizontal microbial transfer, with some inherent limitations.[30] After a week of cohousing to normalize the microbiome in resting conditions, Rag mice were adoptively transferred with 5x10^5 flow-sorted naïve CD4$^+$CD45RB^{HI} T cells. Control Rag mice were injected with sterile PBS as baseline controls. Experimental Rag mice (2 per cage, 6 per group) that had been housed with either Rag or DKO cage-mates were adoptively transferred with T cells. Fecal samples were collected from untreated Rag and DKO cage-mates to monitor the comparative microbiota of each genotype (Fig. 1A). Cage-mates were maintained in the cage to share living quarters and continuously donate fecal matter, but not otherwise studied. All adoptively transferred animals were Rag mice (Fig. S1A). The study continued for 8 weeks post-T cell transfer with weekly longitudinal fecal pellet collection for microbiome study. Comparison of alpha

diversity and composition between groups suggested that the microbiome from DKO mice was not stably established in their cage-mates via horizontal transfer (Fig. 1B and 1C). Despite the dramatically lower alpha diversity of DKO donor mice, Rag mice cohoused with either Rag or DKO mice had a comparable alpha diversity (Fig. 1B). This suggested that the dysbiotic microbiome associated with NHE3-deficiency could not compete by passive exposure in a stable NHE3-competent host. Regardless of the co-housed fecal donors, adoptive transfer with T cells was associated with reductions in the *Lachnospiraceae* family, especially the *Roseburia* genus, and a reciprocal expansion of *Bacteroidaceae* (Fig. 1C and S2), most likely co-occurring with the onset of inflammation.

Despite the failure to gain weight (Fig. 1D), adoptively transferred Rag mice housed with DKO mice did not have significant evidence of enhanced hyperplasia (Fig. 1E) or colonic inflammation (Fig. 1F and S3A) in comparison to Rag mice cohoused with NHE3-competent mice. The colonic mucosa also showed no significant evidence of enhanced expression of inflammatory cytokines by qPCR (Fig. S3B). Thus, lack of passive microbiome sharing between DKO and Rag knockout mice in the cohousing study corresponded with no detectable aggravation of colitis in response to adoptive T cell transfer.

Direct fecal microbiome transplant stably introduces microbial communities from NHE3 sufficient and deficient donors into germ-free mice

We next performed Fecal Microbial Transplant (FMT) from Rag control or DKO fecal donors into germ-free recipients (Fig. S1B). As proof of principle, we first established that the respective microbial communities could be stably transplanted into wildtype germ-

free recipients using oral inoculation. Fecal samples were collected weekly post-association for nine weeks to monitor the microbiome composition. Although DKO fecal donors lacking endogenous NHE3 expression had a more dramatically dysbiotic microbiome composition and lower diversity than the wild-type GF recipients of DKO FMT (Fig. 1A, 2A, and S4A), unweighted Unifrac analysis clearly indicated that different microbiome communities from Rag and DKO mice could be stably introduced to wildtype GF mice (Fig. 2B). While weighted analysis showed that there was some convergence over time in the microbiome (Fig. 2C), taxonomic analysis of individual mice indicated that the major phyla (Fig. 2D) and most bacterial families (Fig. S4B) remained stably different over the course of the nine weeks. The only major exception was the *Bacteroidaceae* family (Fig. 2E), which steadily declined in the wildtype recipients of DKO FMT to eventually reach nearly normal levels observed in the recipients of the control FMT. This observation suggested that perhaps this bacterial family is competitive in the colonic microenvironment fostered in DKO mice, but not under healthy wildtype conditions. Wildtype recipients of FMT from DKO had reduced alpha diversity as compared to the recipients of FMT from control Rag mice (Fig. 2A).

Temporal dynamics and convergence of microbiomes in ex-germ free (ex-GF) Rag mice corresponds with limited pro-inflammatory effect of FMT from NHE3-deficient donors

Having confirmed an efficient establishment of Rag and DKO microbiomes in germ-free wild-type mice, we aimed to determine whether we could reproduce the susceptibility to T-cell mediated colitis we recently reported in adoptively-transferred DKO

mice[26] using microbiome transplant alone, using germ-free (GF) Rag1$^{-/-}$ mice colonized with the dysbiotic microbiota from DKO mice (Fig. S1C). Fresh fecal samples were collected from 4-6 Rag or DKO mice and pooled within each genotype. Fecal slurries were then used to inoculate GF Rag1$^{-/-}$ mice. Germ-free mice that have subsequently been inoculated with microbiota are referred to in this article as ex-germ-free (ex-GF). Following a week of equilibration after inoculation, 5x10^5 of naïve CD4$^+$CD45RB^{HI} T cells were adoptively transferred via i.p. injection to induce colitis. Mice were sacrificed 4.5 weeks post-T cell transfer due to veterinary concern regarding stool consistency and weight loss in selected animals. Beta diversity analysis of the longitudinally collected samples showed that although the DKO FMT recipients' microbiomes remained in a stable dysbiotic state, the T-cell transferred recipients of FMT from control Rag mice began to converge over time toward the dysbiotic DKO microbiome, likely as a result of developing colitis (Fig. 3A). This was most prominent for the major phyla *Bacteroidetes* and *Firmicutes* (Fig. 3B), and driven at the family level by dramatic reductions in SCFA-producing *Firmicutes* families *Lachnospiraceae* and *Ruminococcaceae*, as well as reductions in *Clostridiales vadinBB60*, and a relative expansion of *Bacteroidaceae* (Fig. 3C). Alpha diversity trended lower in recipients of the DKO microbiome, albeit to a lesser extent compared to donors or in the initial experiment with FMT into wildtype GF recipients (Fig. 3D).

Consistent with the convergence of the microbiomes over time, endpoint analysis of colitis at 4.5 weeks after T cell transfer showed only mildly enhanced inflammation in the recipients of DKO microbiome, as compared to the FMT from healthy Rag (Fig. 4 and 5). GF Rag mice that had received FMT from DKO initially lost weight but regained it by

the termination of the experiment (Fig. 4A) and showed a trend towards increased colonic hyperplasia as expressed by colonic weight/length ratio (Fig. 4B). Histology and pathological interpretation indicated that the recipients of FMT from DKO mice had similar trends towards elevated inflammation scores in both proximal and distal colon, however without reaching statistical significance ($p\sim0.08$ for each measure; Fig. 4D-F). Mucosal IL1β was significantly elevated in the recipients of DKO FMT, while expression of TNF, IL-12p40, MMP8 (neutrophil collagenase; surrogate marker of neutrophilic infiltration), and iNOS followed similar trends without reaching statistical significance (Fig. 5A-E).

Immunofluorescence staining for the neutrophil marker Ly6B.2 indicated a significantly elevated influx of neutrophils in the distal colon of DKO microbiota recipients compared to recipients of FMT from Rag mice (Fig. 5F and 5G). There was significantly higher influx of $CD4^+$ cells in the proximal colon, and a positive trend in the distal colon of DKO FMT recipients (Fig. 5F and 5H). Together, these indicate that recipients of the microbiota from DKO mice had a heightened immune response and influx of inflammatory immune cells. Immunofluorescence for cleaved caspase 3 to measure apoptotic cells also indicated a trend toward more cleaved caspase 3 positive cells in the distal colon by cell count, and a significant elevation of staining intensity from cleaved caspase 3 in both segments (Fig. 5F, 5I, and 5J), indicating greater levels of apoptosis among recipients of DKO microbiota.

In conclusion, adoptive naïve T cell transfer into GF $Rag1^{-/-}$ mice associated with Rag or DKO microbiomes showed that DKO microbiome remained in a stable dysbiotic state, whereas the recipients of “healthy” microbiomes of NHE3-competent donors converged over time to resemble aspects of the $NHE3^{-/-}$-like “inflammatory” dysbiosis.

This was driven by dramatic reductions in several anti-inflammatory *Firmicutes* families and a reciprocal expansion of *Bacteroidaceae*, which on a genus level was entirely accounted for by *Bacteroides* (data not shown). Modest inflammatory differences were observed between the two FMT recipients, suggesting greater inflammatory response among recipients of DKO microbiota. However, consistent with the convergence of the microbiomes over time, these differences were nuanced in nature.

The NHE3$^{-/-}$ microbiome remains stably different and promotes accelerated and exacerbated inflammation in the IL-10$^{-/-}$ model of colitis

IL-10$^{-/-}$ mice provide an alternative model of chronic immune-mediated colitis, with obligatory contribution of the microbiota.[31] Introduction of commensal enteric bacteria to germ-free IL-10$^{-/-}$ animals induces progressive colonic inflammation over the course of several weeks. Moreover, colitis in IL-10$^{-/-}$ mice is known to be associated with significant inhibition of NHE3 activity[10], which makes this host more likely to retain the dysbiotic characteristics of DKO microbiome upon colonization. We performed FMT into GF IL-10$^{-/-}$ mice using the fecal slurries from the same pool of donors collected at the same time as the previous fecal transplant experiments to maintain consistency (Fig. S1D). 16S amplicon profiling of the microbiome from IL-10$^{-/-}$ recipients of FMT revealed that in contrast to the adoptive transfer fecal microbiome transplant, the microbiomes of NHE3$^{+/+}$ (Rag) and NHE3$^{-/-}$ (DKO) donors remained stably different in relation to one another over time, although we again observed a noticeable shift in the fecal microbiome of IL10$^{-/-}$ mice receiving Rag microbiome towards convergence at week 7, the final time point (Fig. 6A). At the taxonomic level, however, we observed that although the microbiomes of both

groups changed over time with the onset of disease, they were often changing in parallel (Fig. S5). Again, the onset of inflammation was accompanied in the fecal microbiome by a plummeting abundance of SCFA-producing *Lachnospiraceae*, *Ruminococcaceae*, and *Clostridiales vadinBB60*, and a reciprocal increase in *Bacteroidaceae* (Fig. 6B and S5). In this experiment, recipients of DKO FMT also experienced an increased relative abundance of the *Erysipelotricaceae* family, which has been associated with inflammatory processes (Fig. S5).[30]

At the final time point in the fecal microbiome collection and analysis, the recipients of DKO FMT were still characterized by contractions of overall *Firmicutes* abundance, driven specifically by reductions in *Lachnospiraceae* and *Clostridiales vadinBB60* (Fig. 6B and 6D). The control group also had a higher relative abundance of *Lactobacillaceae* (Fig. 6B and 6D), but a time course analysis suggested that this was a result of an expansion in the control FMT group, not a reduction in the DKO FMT group (Fig. S5). Inflammation was also associated with a dramatic reduction of the *Roseburia* genus, which is part of the *Lachnospiraceae* family and is reduced in human ulcerative colitis[31] and Crohn's disease[32] (Fig. S5). Other reductions in *Lachnospiraceae* and *Ruminococcaceae* genera were also observed (Fig. S5). In this model, we observed a similar trend in reduced alpha diversity in the fecal microbiome of DKO FMT recipients (Fig. 6C).

Considering the consistently observed decrease in SCFA-producing bacteria in both DKO donors and the recipients of the DKO microbiome, we estimated microbial butyrate (butanoate) production using the PICRUSt analysis of function bioinformatics tool. PICRUSt estimates functional pathways utilized by the microbiome based on

community profiling. When comparing an untreated donor population of Rag and DKO mice to IL-10$^{-/-}$ recipients of Rag or DKO microbiota, PICRUSt indicated significant changes in the relative abundance of OTU's associated with butyric acid metabolism (Fig. 6E). Functional profiling also indicated a reduction of OTU's associated with butyrate metabolism among Rag FMT recipients with the onset of inflammation (Fig. 5E).

16S rRNA profiling of the mucosa-adherent bacteria from proximal and distal colonic segments demonstrated that many of the microbiome differences between either Rag and DKO FMT recipients observed in fecal samples were enhanced at the level of the mucosa (Fig. 6). Since they clustered together, for clarity of Fig. 7A, proximal and distal segments are not differentiated by color. DKO FMT recipients were characterized by more dramatic relative reductions of *Firmicutes* driven almost entirely by *Lachnospiraceae* and *Ruminococcaceae* (Fig. 7B and 7C), which are both SCFA-producers and mucin-degraders, and have been shown to be especially sensitive to alkalization of the microenvironment[33]. We observed some gender effect on the mucosal microbiome of the FMT recipients, but these effects, delineated across PC3, did not correspond to inflammatory response which was driven by PC1 (Fig. 7A). While interesting for future study, we have not investigated that question more deeply here. The mucosal microbiome of IL-10$^{-/-}$ recipients of NHE3$^{-/-}$ microbiome had a more noticeable decrease in alpha diversity compared to recipients of Rag FMT (Fig. 7D), in contrast to what we observed in the fecal microbiome from the same experiment (Fig. 6C). Additional functional categories identified by PICRUSt as over- or under-represented in IL-10$^{-/-}$ recipients of Rag or DKO microbiomes are listed in Figure S5 and include modest but significant increase in OTU's associated with bacterial toxins, DNA repair, or

peptidoglycan synthesis, and decrease in categories representing flagellar assembly and bacterial motility (Fig. S6).

GF IL-10$^{-/-}$ mice that had received fecal microbiome from DKO mice had accelerated and mildly exacerbated colitis as compared to those that had received the control microbiome (Fig. 8). The IL-10$^{-/-}$ mice developed severe colitis in recipients of both FMT's, but the inflammation was most severe in the proximal colon of those that received DKO FMT (Fig. 8B). Inflammation scores were not significantly different in the distal colon, though distal colon is typically affected to a lesser degree than cecum and proximal colon in this model. Since FMT recipients from both groups developed severe colitis, and the histological scoring was a point-based system based on percentages of affected segments, the saturation point for pathological scoring was reached in the proximal segment and approached in the distal colon. Thus, we also analyzed as penetrance of disease, where inflammation was expressed as the number of mice exceeding the median of control group (Rag FMT recipients). One hundred percent of DKO FMT recipients exceeded the median of controls in the proximal colon, and the majority also scored higher in the distal colon (Fig. 8C).

To assess the dynamics of colitis development, we analyzed lipocalin 2 (LCN2 or NGAL) levels in longitudinally collected fecal samples. LCN2 is secreted by immune and epithelial cells in response to toll-like receptor (TLR) stimulation to sequester iron and limit bacterial expansion, and has been established as a reliable marker of colitis in mouse models and IBD patients.[32, 33] The increase in LCN2 expression was more rapid in IL-10$^{-/-}$ recipients of DKO FMT, being significantly expressed by 5 weeks (Fig. 8D). The group

that had received control FMT began to catch up at the final collection time, which coincided with the first signs of microbiome convergence (Fig. 6A). An endoscopic analysis from the five-week time point at which the LCN2 levels were significantly different between the two FMT recipient groups showed visible evidence of inflammation in DKO FMT recipients with decreased mucosal transparency, and edema, which were not seen at this time point in the recipients of control microbiome (Fig. 8E). By the final timepoint, when LCN2 levels had caught up in the control group, immunofluorescence indicated a high influx of Ly6B.2^{+} cells (neutrophils), CD4^{+} cells (T cells), and cleaved caspase 3^{+} cells and debris (apoptotic cells) in both groups (Fig. 8F). Recipients of DKO FMT trended toward a higher influx of Ly6B.2^{+} cells in both tissue segments, relatively equal CD4^{+} influx, and significantly higher cleaved caspase 3 activation in the distal colon (Fig. 8F and 8G). These results suggest collectively that the microbiome of NHE3-deficient mice was able to drive a more rapid colonic inflammation in ex-GF IL-10$^{-/-}$ mice.

Together, our data suggest that the microbiota of NHE3-deficient mice has inflammatory potential in germ-free recipients under two different models of experimental colitis, and that this susceptibility is accompanied by consistent loss of SCFA-producing *Firmicutes* and expansion of *Bacteroidaceae*. This suggests a mediating role of NHE3 in shaping the microbiota, and in turn the development of colitis.

DISCUSSION

The paradigm has emerged that diversity and stability of the gut ecosystem is associated with good health, where perturbations to microbial homeostasis and losses of diversity are associated with a variety of disease processes.[36] Inflammatory bowel diseases are associated with losses in microbiome diversity, with relative expansion of *Proteobacteria* and contraction of the *Firmicutes* phylum.[37-39] These losses include butyrate-producing microbes associated with the members of the *Lachnospiraceae* and *Ruminococcaceae* families,[40,41] such as *Faecalibacterium prausnitzii.*[42,43] These changes in microbial gut ecology, frequently referred to as dysbiosis, are now widely considered as an important environmental factor contributing to the pathogenesis of IBD. The importance of dysbiosis as a causative or modulating factor of the history of the disease is still not clear, as are dietary or host-related factors that lead to instability of the gut microbiome. Our previous findings pointed at the role of impaired apical Na^+/H^+ exchange as a likely mechanism contributing to microbial dysbiosis. This membrane transport is mediated by three antiporters, NHE2, NHE3, and NHE8, with subtle differences in colonic expression pattern. The latter two are inhibited in animal models of IBD,[9-11] as well as in human patients,[11, 34, 35] and deletion of NHE3 in mice was sufficient to lead to microbiome changes similar to that observed in human IBD,[22] microbiota-dependent spontaneous colitis,[20] and increased susceptibility to mucosal injury or T-cell mediated colitis.[21, 26] These observations prompted us to hypothesize that impaired Na^+/H^+ exchange, be it the result of initial subclinical inflammation or infection, lead to microbial dysbiosis, which in turn lowers the inflammatory threshold or otherwise modulates mucosal immune responses.

We first tested the ability of the dysbiotic microbial community to horizontally transfer into healthy Rag2$^{-/-}$ mice by co-housing them with Rag2$^{-/-}$ or DKO mice, followed by adoptive T cell transfer. In this approach, we showed that dysbiosis established in NHE3-deficient mice is not dominant and does not transfer into an NHE3-sufficient host. Consistent with this observation, we did not observe different susceptibility to adoptive T cell transfer in Rag mice co-housed with DKO mice. Using GF untreated WT mice, we were able to effectively transplant and maintain dysbiotic community from DKO mice. However, T cell transfer colitis in similarly associated Rag mice led to inflammation-induced convergence of the microbial ecology in the recipients of Rag and DKO microbiomes, and the end-point analysis of colonic inflammation showed only modest effect of the FMT, again suggesting that in a scenario where microbiome merges in the new host to represent more similar composition, the effect of FMT from NHE3-deficient donors is minor. To overcome this experimental confounder, we turned to IL-10$^{-/-}$ mice, a strain known not only for strict microbial dependence in colitis susceptibility, but also for inhibition of NHE3 activity.[10] Here, we observed accelerated disease development, with the largest difference between recipient IL-10$^{-/-}$ mice seen at 5 weeks post-colonization. This observation suggested that gut microbiome shaped by disrupted Na^+/H^+ exchange can modulate the time of disease onset and its severity. Incidentally, early and adolescent IBD was reported in a subset of patients with a rare genetic disorder, congenital sodium diarrhea, associated with inactivating mutations of NHE3.[36]

Lachnospiraceae and *Ruminococcaceae*, also commonly known as *Clostridia* clusters XIVa and IV respectively, are fairly abundant members of the normal microbiome, reaching approximately 10-20% of abundance in healthy humans where they break down

indigestible carbohydrates and produce short chain fatty acids (SCFA) such as butyrate.[37] Both are negatively affected in NHE3-deficient mice, which may be correlated with decreased microbial production of SCFA's, which serve as the primary energy fuel for colonocytes and exert immunomodulatory roles in the gut mucosa. These taxa are also some of the most significantly different in the IL-10$^{-/-}$ recipients of the microbiome from NHE3-sufficient and –deficient donors. Many of these family members, notably *Roseburia* spp., which was also vulnerable to inflammation in our model, largely reside in the mucus layer of the intestine.[38] This localization may make them particularly vulnerable to microenvironmental changes brought about by disruptions in sodium hydrogen exchange. NHE3, which brings in luminal sodium in exchange for cellular hydrogen, helps facilitate a pH gradient at the brush border as protons diffuse out of the unstirred layer. This gradient is important for mucin structure, which exists in a compact impenetrable layer at the lowest pH next to the epithelia, and expands with the rising pH to form the secondary mucus layer that is widely inhabited and consumed by the microbiota.[18, 39, 40] Indeed, we and others showed that NHE3 deficiency is associated with bacterial encroachment upon the brush border membrane and increased bacterial translocation.[19, 20]

Changes in pH have also been shown to have consequences on *Lachnospiraceae* and *Ruminococcaceae* families as well as SCFA production. A change from a pH of 5.5 to 6.5 dramatically stunted both bacterial abundance as well as butyrate production – shifting instead to a peak production of propionate and an expansion of *Bacteroides.*[41]

SCFA, and especially butyrate, are potent positive regulators of NHE3 expression and activity.[42, 43] Therefore, decreased relative abundance of *Lachnospiraceae* and *Ruminococcaceae* families along with colonic SCFA production in NHE3-deficient mice

suggests an existence of a positive feedback mechanism whereby butyrate producers promote stable expression and activity of NHE3, which sustains acidic mucosal milieu to sustain a competitive advantage to these and other acidophilic bacteria.

In addition to the contraction of *Lachnospiraceae* and *Ruminococcaceae*, NHE3 deficiency and inflammation are consistently associated with the expansion of *Bacteroidaceae* in our model. When sequencing resolution allowed, this expansion was determined to belong exclusively to the *Bacteroides* genera (data not shown). *Bacteroidaceae* taxa have been associated with colitis, with *Bacteroides* inducing colitis in a susceptible animal model.[24] *Bacteroidaceae* is also reported to expand following ablation of nucleotide-binding oligomerization domain-containing protein 2 (NOD2), which mediates mucosal homeostasis and is one of the major allelic mutations associated with IBD.[44] The dextran-sodium sulfate (DSS) injury model of colitis also dramatically promoted *Bacteroidaceae* family expansion.[45] The species *Bacteroides thetaiotamicron,* a known pathobiont, is reportedly expanded in NHE3$^{-/-}$ mice,[23-25] although our sequencing depth did not allow us to verify whether this species was responsible. Alongside our data, in which *Bacteroidaceae* expansion follows both NHE3 deficiency and the onset of disease, it is possible that the family is both competitive under circumstances that promote mucosal inflammation, and potentially a cause of enhanced colitis. It is therefore possible that the inflammatory potential mediated by the NHE3-deficient microbiome is not strictly due to reduced SCFA production, but also the expansion of a pathobiont which favors an inflammatory milieu. Moreover, *Bacteroidaceae* benefit from the same elevation in pH that is detrimental to *Lachnospiraceae and Ruminococcaceae*[41], suggesting a trade-off that is potentially directly mediated by NHE3.

One exceptional *Firmicute* is *Clostridium difficile*, the pathobiont responsible for the epidemic of hospital related diarrhea, which is adapted to replicate optimally at a slightly higher pH than other *Clostridia* species.[46] *C. difficile* reduces NHE3 activity,[16] and the resulting pH change may give it a competitive advantage.[46] Reciprocally, *Lachnospiraceae* alone are capable of promoting resistance to *C. difficile,*[47] perhaps by the opposing effect on pH through SCFA production. This ongoing standoff is supported by the observation that our IL-10$^{-/-}$ recipients of NHE3$^{-/-}$ FMT had an expansion of *Peptostreptococcaceae,* which houses *Clostridium difficile*, though our compositional studies did not allow for species-level resolution. It is plausible that species within the *Bacteroidaceae* family display similar competitive properties.

In summary, our current and previously reported findings show that NHE3 activity is a strong determinant of stable eubiotic gut microbiome. While the contribution of NHE3 to mucosal homeostasis is likely complex and multifactorial, despite the inherent methodological difficulties, we could demonstrate that disrupted apical Na^+/H^+ exchange contributes to the timing and severity of intestinal inflammation at least in part through modulation of the gut microbial ecology and decreased synthesis of SCFA's.

Methods

Mice

Ethics Statement

All animals used in the experiments that were carried out at the University of Arizona were handled in accordance with University of Arizona University Animal Care (UAC) guidelines and with approved IACUC protocol (Kiela). IL-10$^{-/-}$ mouse experiments were conducted in collaboration with the University of Florida, and all animals therein were handled according to an approved University of Florida IACUC protocol (Jobin).

Co-Housing Followed by Adoptive T Cell Transfer

Rag2$^{-/-}$ mice (Rag) on a 129SvEv background were either housed with Rag or NHE3xRag2$^{-/-}$ (DKO) donors at a ratio of 2:3 Rag:donors. Littermates serving as donors were not manipulated, and only existed to share living space and donate fecal matter to the experimental Rag mice (n=2 experimental mice per cage, 3 cages, n=6 per group). All mice in this experiment were female to facilitate cohousing while avoiding aggression in minimize the influence of stress. Animals were cohoused for one week prior to adoptive transfer with naïve T cells or PBS. Mice were weighed and fecal samples were collected weekly. Littermate DKO mice that died during the course of the experiment were promptly replaced by another double knockout to keep the 2:3 ratio. Experimental mice were kept for eight weeks before sacrifice.

Fecal Microbiome Transplant into Wildtype Germ-free Mice

Fecal slurries were prepared from Rag and DKO mice. Wild-type (WT) germ-free mice on C57BL/6 genetic background were orally inoculated with one of the slurries and followed for 9 weeks, with weekly fecal sample collections. At the end of 9 weeks, mice were sacrificed and fecal samples were processed for fecal microbiome analysis.

Fecal Microbiome Transplant into Germ-free Rag$^{-/-}$ Followed by Adoptive T Cell Transfer

Fecal slurries were prepared from Rag and DKO donors. Germ-free Rag1$^{-/-}$ C57BL/6 mice were inoculated with fecal slurries from Rag or DKO mice (n=6 per group). Ex-GF mice were subsequently allowed to habituate for a week before adoptive transfer with $CD4^{+}CD45RB^{HI}$ T cells. Mice were weighed weekly, and fecal samples collected weekly. After a little over four weeks, animals were sacrificed at the request of the veterinary personnel, and tissues were processed.

Fecal Microbiome Transplant into Germ-free IL-10$^{-/-}$ *Mice*

These experiments were done in collaboration with the University of Florida. All animals were handled in the University of Florida gnotobiotic animal facility. Fecal samples for the creation of donor slurries were collected and shipped frozen to Florida for fresh slurry preparation. Germ-free IL-10$^{-/-}$ mice were inoculated with either Rag or DKO slurry. Animals were weighed weekly, and fecal samples were collected at day 0, and weeks 2, 4, 5 and 7. Additional fecal samples were collected at 2, 5, and 7 weeks for Lipocalin 2 ELISA (R&D Systems, Bio-Techne Corporation, Minneapolis, MN). At 7

weeks, the experiment was completed, animals sacrificed and tissues shipped frozen to the University of Arizona for analysis.

Histology and Pathological Interpretation

Histological preparations were done by the University of Arizona University Animal Care (UAC) Pathology Services core. Pathological interpretation and inflammation scoring was performed by an experienced veterinary pathologist (D. Besselsen; UAC) blinded to the experimental design and sample group assignment. For more detail, see Supplemental Methods section.

Immunofluorescence and Cell Quantitation

Tissue sections were analyzed by immunofluorescence for Ly6B.2, CD4, and cleaved caspase 3. Slides were de-paraffinized and hydrated, followed by antigen retrieval, blocking, and staining with primary and secondary antibody. Below is a table of the antibodies/dilutions used. For greater detail, refer to the supplemental methods section.

Primary Ab	Species & Secondary	Company/Cat #	Dilution
Ly6B.2	Rat anti mouse alloantigen 1°	Biorad MCA771GT	1:1000
	647 Chicken anti Rat IgG 2°	Life Technologies A21472	1:1000
CD4	Rabbit anti mouse recombinant 1°	Abcam ab183685	1:500
	647 Goat anti rabbit 2°	Life Technologies A21246	1:400
Cleaved Caspase 3	Rabbit anti mouse mAb 1°	Cell Signaling Technologies D175	1:1000
	647 Goat anti rabbit 2°	Life Technologies A21246	1:1000

Cells were quantified using Fiji/Image J. Multiple representative images were collected from each slide at 200x magnification, and file names blinded for analysis. For Ly6B.2 and CD4, which are surface markers, single-channel (Cy5) images were counted using the multi-point tool in Fiji, using overlaid images for reference if needed. Because cleaved caspase 3 is an apoptosis marker, making cell counting ambiguous at times, we both did a cell count and additionally measured pixel intensity per field of vision, where field of vision refers to the part of the slide occupied by tissue. Analysis was also blinded for pixel intensity counts. After all images had been counted, files were unblinded and analyzed by group.

Adoptive T Cell Transfer

Adoptive transfer of naïve $CD4^{+}CD45RB^{HI}$ T cells was carried out as described and previously performed.[26] For more detail, see Supplemental Methods section.

Fecal Microbiome Transplant

Fecal samples were collected from untreated 129SvEv $Rag2^{-/-}$ (Rag) and NHE3x$Rag2^{-/-}$ (DKO) donors. Donor fecal pellets were collected at the same time from the same donors, stored at -80°C until use, and prepared fresh the day of inoculation. On the day of inoculation, fecal samples were made into a slurry of 200 mg/ml fecal matter using sterile PBS. Slurries were promptly carried down to the animal facility on ice, where they were used to inoculate recipient mice by introducing the slurries to the oral cavity and fur (200μl slurry per mouse). Germ-free animals were inoculated once.

Fecal microbial DNA extraction

Fecal samples were collected and stored at -80°C until use. DNA was extracted in 96-well format using the DNeasy PowerSoil HTP 96 Kit (Qiagen, formerly MoBio) according to the manufacturer protocol.

Mucosal DNA and RNA extraction

Mucosal DNA and RNA were isolated from colonic segments using the AllPrep DNA/RNA Mini Kit (Qiagen, cat # 80204) with a modified protocol described in more detail in the Supplemental Methods section.

Next-Generation Sequencing

The V4 fragments of 16S rRNA gene from extracted fecal and mucosal DNA were sequenced using an Illumina MiSeq platform. More detail on library construction and sequencing is provided in the Supplemental Methods section.

Bioinformatic Analysis of the Microbiome

Bioinformatic analysis of sequenced amplicons was performed using the QIIME 1.9.1 software package, a Python-based, open-source command-line package developed for the analysis of microbial datasets. PICRUSt v. 1.1.1 (Phylogenetic Investigation of Communities by Reconstruction of Unobserved States) was used to predict metagenome

functional content based on the marker gene, 16S rRNA gene surveys. More detail on the bioinformatics analysis of the data is provided in the Supplemental Methods section.

Quantitative RT-PCR

Following RNA-extraction (described above), mucosal RNA from proximal and distal segments was quantified and reverse-transcribed into cDNA (Bioline, cat # BIO-65054). Quantitative real-time PCR (qRT-PCR) was performed in 10μl reactions using Bioline mastermix (cat # BIO-86005) and FAM-conjugated probes for relevant cytokines and targets (Applied Biosystems). Cq values were obtained using the LightCycler96 thermocycler (Roche) and the LightCycler96 software (version 1.1.0.1320). Raw Cq values were exported to Microsoft Excel and the gene expression changes to experimental controls, using GAPDH as the housekeeping gene.

Fecal SCFA and Lipocalin-2 detection

SCFA analyses were performed by Creative proteomics, a Division of Creative Dynamics, Inc. (Shirley, NY) using reverse phase ultra-performance liquid chromatographic (UPLC) method described in detail in the Supplemental Methods section. Lipocalin 2 was detected by ELISA (R&D Systems, Bio-Techne Corporation, Minneapolis, MN) as described in the Supplemental Methods section.

Statistical Analysis

Statistical analyses of non-microbiome data were performed using GraphPad Prism Version 7.00. Unless otherwise indicated, comparisons of two groups in which both groups passed a Shapiro-Wilke normality test were compared by two-tailed Student t-test. Those in which one or both groups did not pass a Shapiro Wilke normality test were compared by a non-parametric Mann-Whitney U-test. For comparison of three or more groups, if three or more groups passed the Shapiro-Wilke normality test, standard ANOVA was used with a Fisher LSD post hoc test. In cases where two or more groups failed a Shapiro Wilke normality test, groups were compared by non-parametric Kruskal-Wallis test with Dunn's multiple comparison's test.

Acknowledgements

This work was supported by the National Institute of Diabetes and Digestive and Kidney Diseases Grants 2R01DK041274 (to F. Ghishan and P. Kiela) and 5R01DK073338 (to C. Jobin). The founders had no role in study design, data collection and analysis, decision to publish, or preparation of the manuscript. Special thanks to Paula Campbell with the University of Arizona Flow Cytometry Core for her assistance flow sorting T cells for adoptive transfer.

Author Contributions

C.A.H. designed and performed experiments, analyzed results, and wrote the paper; D.L. performed experiments, analyzed results, and edited the paper; C.L.O. designed and performed experiments with germ-free IL-10$^{-/-}$ mice; M.T.M-K., responsible for most experimental animals, performed experiments; K.P. designed and performed experiments with germ-free mice in Arizona; D.G.B. analyzed histology and scored samples; D.R.J. performed flow sorting of T cells; C.J. supervised experiments with germ-free IL-10$^{-/-}$ mice at the Univ. of Florida, provided funding, edited manuscript; F.K.G. supervised experiments at the Univ. of Arizona, provided funding, edited manuscript; P.R.K. supervised experiments at the Univ. of Arizona, designed the experiments, analyzed results provided funding, edited manuscript.

References

1. Coskun M. Intestinal epithelium in inflammatory bowel disease. *Front Med (Lausanne)* 2014; **1:** 24.

2. Ghishan FK, Kiela PR. Epithelial transport in inflammatory bowel diseases. *Inflamm Bowel Dis* 2014; **20**(6)**:** 1099-1109.

3. Kiela PR, Xu H, Ghishan FK. Apical NA+/H+ exchangers in the mammalian gastrointestinal tract. *J Physiol Pharmacol* 2006; **57 Suppl 7:** 51-79.

4. Gurney MA, Laubitz D, Ghishan FK, Kiela PR. Pathophysiology of Intestinal Na+/H+ exchange. *Cell Mol Gastroenterol Hepatol* 2017; **3**(1)**:** 27-40.

5. Schultheis PJ, Clarke LL, Meneton P, Miller ML, Soleimani M, Gawenis LR *et al.* Renal and intestinal absorptive defects in mice lacking the NHE3 Na+/H+ exchanger. *Nat Genet* 1998; **19**(3)**:** 282-285.

6. Clayburgh DR, Musch MW, Leitges M, Fu YX, Turner JR. Coordinated epithelial NHE3 inhibition and barrier dysfunction are required for TNF-mediated diarrhea in vivo. *J Clin Invest* 2006; **116**(10)**:** 2682-2694.

7. Amin MR, Malakooti J, Sandoval R, Dudeja PK, Ramaswamy K. IFN-gamma and TNF-alpha regulate human NHE3 gene expression by modulating the Sp family transcription factors in human intestinal epithelial cell line C2BBe1. *Am J Physiol Cell Physiol* 2006; **291**(5)**:** C887-896.

8. Rocha F, Musch MW, Lishanskiy L, Bookstein C, Sugi K, Xie Y *et al.* IFN-gamma downregulates expression of Na(+)/H(+) exchangers NHE2 and NHE3 in rat intestine and human Caco-2/bbe cells. *Am J Physiol Cell Physiol* 2001; **280**(5)**:** C1224-1232.

9. Barmeyer C, Harren M, Schmitz H, Heinzel-Pleines U, Mankertz J, Seidler U *et al.* Mechanisms of diarrhea in the interleukin-2-deficient mouse model of colonic inflammation. *Am J Physiol Gastrointest Liver Physiol* 2004; **286**(2)**:** G244-252.

10. Lenzen H, Lunnemann M, Bleich A, Manns MP, Seidler U, Jorns A. Downregulation of the NHE3-binding PDZ-adaptor protein PDZK1 expression during cytokine-induced inflammation in interleukin-10-deficient mice. *PLoS One* 2012; **7**(7)**:** e40657.

11. Sullivan S, Alex P, Dassopoulos T, Zachos NC, Iacobuzio-Donahue C, Donowitz M *et al.* Downregulation of sodium transporters and NHERF proteins in IBD patients and mouse colitis models: potential contributors to IBD-associated diarrhea. *Inflamm Bowel Dis* 2009; **15**(2)**:** 261-274.

12. Siddique I, Hasan F, Khan I. Suppression of Na+/H+ exchanger isoform-3 in human inflammatory bowel disease: lack of reversal by 5'-aminosalicylate treatment. *Scand J Gastroenterol* 2009; **44**(1)**:** 56-64.

13. Yeruva S, Farkas K, Hubricht J, Rode K, Riederer B, Bachmann O *et al.* Preserved Na(+)/H(+) exchanger isoform 3 expression and localization, but decreased NHE3 function indicate regulatory sodium transport defect in ulcerative colitis. *Inflamm Bowel Dis* 2010; **16**(7)**:** 1149-1161.

14. Farkas K, Yeruva S, Rakonczay Z, Jr., Ludolph L, Molnar T, Nagy F *et al.* New therapeutic targets in ulcerative colitis: the importance of ion transporters in the human colon. *Inflamm Bowel Dis* 2011; **17**(4)**:** 884-898.

15. Subramanya SB, Rajendran VM, Srinivasan P, Nanda Kumar NS, Ramakrishna BS, Binder HJ. Differential regulation of cholera toxin-inhibited Na-H exchange isoforms by butyrate in rat ileum. *Am J Physiol Gastrointest Liver Physiol* 2007; **293**(4)**:** G857-863.

16. Hayashi H, Szaszi K, Coady-Osberg N, Furuya W, Bretscher AP, Orlowski J *et al.* Inhibition and redistribution of NHE3, the apical Na+/H+ exchanger, by Clostridium difficile toxin B. *J Gen Physiol* 2004; **123**(5)**:** 491-504.

17. Hodges K, Alto NM, Ramaswamy K, Dudeja PK, Hecht G. The enteropathogenic Escherichia coli effector protein EspF decreases sodium hydrogen exchanger 3 activity. *Cell Microbiol* 2008; **10**(8)**:** 1735-1745.

18. Ambort D, Johansson ME, Gustafsson JK, Nilsson HE, Ermund A, Johansson BR *et al.* Calcium and pH-dependent packing and release of the gel-forming MUC2 mucin. *Proc Natl Acad Sci U S A* 2012; **109**(15)**:** 5645-5650.

19. Johansson ME, Gustafsson JK, Holmen-Larsson J, Jabbar KS, Xia L, Xu H *et al.* Bacteria penetrate the normally impenetrable inner colon mucus layer in both murine colitis models and patients with ulcerative colitis. *Gut* 2014; **63**(2)**:** 281-291.

20. Laubitz D, Larmonier CB, Bai A, Midura-Kiela MT, Lipko MA, Thurston RD *et al.* Colonic gene expression profile in NHE3-deficient mice: evidence for spontaneous distal colitis. *Am J Physiol Gastrointest Liver Physiol* 2008; **295**(1)**:** G63-G77.

21. Kiela PR, Laubitz D, Larmonier CB, Midura-Kiela MT, Lipko MA, Janikashvili N *et al.* Changes in mucosal homeostasis predispose NHE3 knockout mice to increased susceptibility to DSS-induced epithelial injury. *Gastroenterology* 2009; **137**(3)**:** 965-975, 975 e961-910.

22. Larmonier CB, Laubitz D, Hill FM, Shehab KW, Lipinski L, Midura-Kiela MT *et al.* Reduced colonic microbial diversity is associated with colitis in NHE3-deficient mice. *Am J Physiol Gastrointest Liver Physiol* 2013; **305**(10)**:** G667-677.

23. Engevik MA, Aihara E, Montrose MH, Shull GE, Hassett DJ, Worrell RT. Loss of NHE3 alters gut microbiota composition and influences Bacteroides thetaiotaomicron growth. *Am J Physiol Gastrointest Liver Physiol* 2013; **305**(10)**:** G697-711.

24. Bloom SM, Bijanki VN, Nava GM, Sun L, Malvin NP, Donermeyer DL *et al.* Commensal Bacteroides species induce colitis in host-genotype-specific fashion in a mouse model of inflammatory bowel disease. *Cell Host Microbe* 2011; **9**(5)**:** 390-403.

25. Hansen JJ, Huang Y, Peterson DA, Goeser L, Fan TJ, Chang EB *et al.* The colitis-associated transcriptional profile of commensal Bacteroides thetaiotaomicron enhances adaptive immune responses to a bacterial antigen. *PLoS One* 2012; **7**(8)**:** e42645.

26. Laubitz D, Harrison CA, Midura-Kiela MT, Ramalingam R, Larmonier CB, Chase JH *et al.* Reduced Epithelial Na+/H+ Exchange Drives Gut Microbial Dysbiosis and Promotes Inflammatory Response in T Cell-Mediated Murine Colitis. *PLoS One* 2016; **11**(4)**:** e0152044.

27. Du Z, Hudcovic T, Mrazek J, Kozakova H, Srutkova D, Schwarzer M *et al.* Development of gut inflammation in mice colonized with mucosa-associated bacteria from patients with ulcerative colitis. *Gut Pathog* 2015; **7:** 32.

28. Garrett WS, Lord GM, Punit S, Lugo-Villarino G, Mazmanian SK, Ito S *et al.* Communicable ulcerative colitis induced by T-bet deficiency in the innate immune system. *Cell* 2007; **131**(1)**:** 33-45.

29. Soave O, Brand CD. Coprophagy in animals: a review. *Cornell Vet* 1991; **81**(4)**:** 357-364.

30. Laukens D, Brinkman BM, Raes J, De Vos M, Vandenabeele P. Heterogeneity of the gut microbiome in mice: guidelines for optimizing experimental design. *FEMS Microbiol Rev* 2016; **40**(1)**:** 117-132.

31. Sellon RK, Tonkonogy S, Schultz M, Dieleman LA, Grenther W, Balish E *et al.* Resident enteric bacteria are necessary for development of spontaneous colitis and immune system activation in interleukin-10-deficient mice. *Infect Immun* 1998; **66**(11)**:** 5224-5231.

32. Chassaing B, Srinivasan G, Delgado MA, Young AN, Gewirtz AT, Vijay-Kumar M. Fecal lipocalin 2, a sensitive and broadly dynamic non-invasive biomarker for intestinal inflammation. *PLoS One* 2012; **7**(9)**:** e44328.

33. Buisson A, Vazeille E, Minet-Quinard R, Goutte M, Bouvier D, Goutorbe F *et al.* Fecal Matrix Metalloprotease-9 and Lipocalin-2 as Biomarkers in Detecting Endoscopic Activity in Patients With Inflammatory Bowel Diseases. *J Clin Gastroenterol* 2017.

34. Li X, Cai L, Xu H, Geng C, Lu J, Tao L *et al.* Somatostatin regulates NHE8 protein expression via the ERK1/2 MAPK pathway in DSS-induced colitis mice. *Am J Physiol Gastrointest Liver Physiol* 2016; **311**(5)**:** G954-G963.

35. Yeruva S, Chodisetti G, Luo M, Chen M, Cinar A, Ludolph L *et al.* Evidence for a causal link between adaptor protein PDZK1 downregulation and Na(+)/H(+) exchanger NHE3 dysfunction in human and murine colitis. *Pflugers Arch* 2015; **467**(8)**:** 1795-1807.

36. Janecke AR, Heinz-Erian P, Muller T. Congenital Sodium Diarrhea: A Form of Intractable Diarrhea, With a Link to Inflammatory Bowel Disease. *J Pediatr Gastroenterol Nutr* 2016; **63**(2)**:** 170-176.

37. Pryde SE, Duncan SH, Hold GL, Stewart CS, Flint HJ. The microbiology of butyrate formation in the human colon. *FEMS Microbiol Lett* 2002; **217**(2)**:** 133-139.

38. Van den Abbeele P, Belzer C, Goossens M, Kleerebezem M, De Vos WM, Thas O *et al.* Butyrate-producing Clostridium cluster XIVa species specifically colonize mucins in an in vitro gut model. *ISME J* 2013; **7**(5)**:** 949-961.

39. Johansson ME, Larsson JM, Hansson GC. The two mucus layers of colon are organized by the MUC2 mucin, whereas the outer layer is a legislator of host-microbial interactions. *Proc Natl Acad Sci U S A* 2011; **108 Suppl 1:** 4659-4665.

40. Johansson ME, Phillipson M, Petersson J, Velcich A, Holm L, Hansson GC. The inner of the two Muc2 mucin-dependent mucus layers in colon is devoid of bacteria. *Proc Natl Acad Sci U S A* 2008; **105**(39)**:** 15064-15069.

41. Walker AW, Duncan SH, McWilliam Leitch EC, Child MW, Flint HJ. pH and peptide supply can radically alter bacterial populations and short-chain fatty acid ratios within microbial communities from the human colon. *Appl Environ Microbiol* 2005; **71**(7)**:** 3692-3700.

42. Kiela PR, Kuscuoglu N, Midura AJ, Midura-Kiela MT, Larmonier CB, Lipko M *et al.* Molecular mechanism of rat NHE3 gene promoter regulation by sodium butyrate. *Am J Physiol Cell Physiol* 2007; **293**(1)**:** C64-74.

43. Musch MW, Bookstein C, Xie Y, Sellin JH, Chang EB. SCFA increase intestinal Na absorption by induction of NHE3 in rat colon and human intestinal C2/bbe cells. *Am J Physiol Gastrointest Liver Physiol* 2001; **280**(4)**:** G687-693.

44. Couturier-Maillard A, Secher T, Rehman A, Normand S, De Arcangelis A, Haesler R *et al.* NOD2-mediated dysbiosis predisposes mice to transmissible colitis and colorectal cancer. *J Clin Invest* 2013; **123**(2)**:** 700-711.

45. Berry D, Kuzyk O, Rauch I, Heider S, Schwab C, Hainzl E *et al.* Intestinal Microbiota Signatures Associated with Inflammation History in Mice Experiencing Recurring Colitis. *Front Microbiol* 2015; **6:** 1408.

46. Engevik MA, Engevik KA, Yacyshyn MB, Wang J, Hassett DJ, Darien B *et al.* Human Clostridium difficile infection: inhibition of NHE3 and microbiota profile. *Am J Physiol Gastrointest Liver Physiol* 2015; **308**(6)**:** G497-509.

47. Reeves AE, Koenigsknecht MJ, Bergin IL, Young VB. Suppression of Clostridium difficile in the gastrointestinal tracts of germfree mice inoculated with a murine isolate from the family Lachnospiraceae. *Infect Immun* 2012; **80**(11)**:** 3786-3794.

FIGURE LEGENDS

Figure 1. **Passive microbiome sharing (cohousing) is inefficient and does not confer susceptibility to colitis.** Rag mice were cohoused with either other Rag2$^{-/-}$ or DKO (NHE3xRag2$^{-/-}$ double knockout) littermates in a 2:3 ratio Rag:donor. Rag mice (2 per cage, 6 per group) were adoptively transferred with 0.5x10^5 naïve CD4$^+$CD45RB^{hi} T cells or injected with sterile PBS (control). Fecal samples were collected weekly for microbiome analysis. **A**. A family level microbiome composition for Rag and DKO fecal donors as a reference. **B**. Alpha diversity analysis depicting observed OTUs between Rag or DKO fecal donors (D=donor) and in co-housed Rag mice either adoptively transferred with naive T cells or injected with PBS. **C**. Family-level taxonomic composition at weekly time points in Rag mice co-housed with NHE3$^{+/+}$ Rag mice or with NHE3$^{-/-}$ Rag mice, with adoptive T cell transfer or injected with PBS. **D**. Percent weight change, measured weekly, among recipient Rag mice. T cell-transferred Rag mice cohoused with DKO mice lost more weight than those co-housed with DKO (*). Among PBS-injected Rag mice, those co-housed with DKO mice tended to have lower body weight than those co-housed with Rag mice (#) (two-way ANOVA). **E**. Colonic hyperplasia of Rag mice as measured weight/length ratio at sacrifice. **F**. Histological inflammation score as measured by a pathologist blinded to experimental design.

Figure 2. **NHE3$^{+/+}$ and NHE3$^{-/-}$ microbiomes are stably transferrable to germ-free WT recipients.** Fecal microbiome transplant (FMT) from Rag (NHE3$^{+/+}$) or DKO (NHE3xRag2$^{-/-}$ double knockout) mice into wildtype germ-free mice. Mice were maintained for nine weeks post-colonization with weekly fecal collections (w1 to w9). **A**. Alpha rarefaction plot depicting observed OTUs from wildtype mice that had received FMT from either Rag (blue) or DKO (red) donors. **B**. Principal coordinate analysis depicting beta diversity over time in an unweighted UNIFRAC analysis. **C**. Principal coordinate analysis depicting the beta diversity over time in a weighted UNIFRAC analysis, which takes into account the abundance of each taxa in its calculation. **D**. Relative abundance (% of total) of *Bacteroidetes* and *Firmicutes* in GF wildtype mice inoculated with Rag or DKO microbiota. **E.** Relative abundance (% of total) of *Bacteroidaceae* family over time in GF wildtype mice inoculated with Rag or DKO microbiota. * $p<0.05$, ** $p<0.01$, *** $p<0.001$. Two-Way ANOVA.

Figure 3. **Convergence of microbiomes of the FMT recipients during inflammation in adoptive T cell transfer.** Germ-free Rag mice were colonized with microbiome from either Rag or DKO (NHE3xRag2$^{-/-}$) mice. All mice were adoptively transferred with 0.5x10^5 naïve CD4$^+$CD45RB^{hi} T cells 7 days later. Time points (weekly) are shown in reference to the time

of inoculation. **A**. (Upper panel) Principal coordinate analysis depicting beta diversity (unweighted UNIFRAC) over time in Rag recipients of Rag or DKO FMT. Single, unconnected blue and red dots represent the Rag and DKO donors, respectively; (lower panel) alpha rarefaction plot depicting the alpha diversity shown as observed OTUs in Rag recipients of FMT from either Rag (blue) or DKO (red) fecal donors **B**. relative abundance of the two main bacterial phyla, *Bacteroidetes* and *Firmicutes* among the two FMT groups. **C**. Relative abundance of selected families among Rag recipients of FMT from either Rag or DKO donors. * $p<0.05$, ** $p<0.01$, *** $p<0.001$. Two-Way ANOVA.

Figure 4. Microbiota convergence diminishes the differences in inflammatory response to adoptive T cell transfer in ex-GF Rag mice.

A. Relative body weight loss, measured weekly, in Rag recipients of Rag or DKO (NHE3xRag2$^{-/-}$) FMT after adoptive T cell transfer. **B**. Colonic hyperplasia in Rag recipients of the respective FMT, expressed as mg/cm of the colon at sacrifice. **C**. Representative H&E stained proximal and distal colonic sections from Rag recipients of FMT (100X magnification). **D**. Proximal, **E**. distal, and **F**. combined histological inflammation scores.

Figure 5. **Increased cytokine expression and immune infiltration in the recipients of DKO FMT after adoptive naïve T cell transfer.**

A-E. RT-qPCR assessment of colonic expression of selected inflammatory mediators. Data analyzed by Student T-test, p values indicated in graph. **F.** Immunofluorescence imaging of Ly6B.2^{+}, CD4^{+}, and cleaved caspase 3^{+} cells as seen in proximal and distal colonic sections (200x magnification). **G-I.** Quantitation of Ly6B.2^{+}, CD4^{+}, and cleaved caspase 3^{+} cells by colonic segment as counted in Image J by blinded analysis. **J**. Pixel intensity per field of vision for cleaved caspase 3, as an apoptotic marker, calculated by Image J in a blinded analysis. **G-J**. * $p<0.05$, ** $p<0.01$, *** $p<0.001$, **** $p<0.0001$.

Figure 6. Fecal microbiota of germ-free IL-10$^{-/-}$ mice colonized with microbial community from Rag of DKO mice remain stably different over time. GF IL-10$^{-/-}$ mice were colonized with fecal microbiome from either Rag or DKO (NHE3xRag2$^{-/-}$) donors and maintained for seven weeks, with prospective fecal collection. **A.** Principal coordinate analysis showing beta diversity over time (unweighted UNIFRAC) in IL-10$^{-/-}$ recipients of FMT from Rag (blue) or DKO (red) mice. **B.** Family-level microbiome composition bar charts depicting the fecal microbiomes at sacrifice in IL-10$^{-/-}$ recipients of Rag (Rag $\rightarrow$ IL-10$^{-/-}$) or DKO (DKO $\rightarrow$ IL-10$^{-/-}$) microbiome. **C.** Alpha-rarefaction plot depicting alpha diversity shown in observed OTUs of the fecal microbiome between IL-10$^{-/-}$ recipients of Rag (blue) or DKO (red) FMT. **D**. Relative abundance of selected bacterial families from IL-10$^{-/-}$

recipients of FMT measured at sacrifice (week 7). * $p<0.05$, ** $p<0.01$, Mann-Whitney U-test. **E.** Ontology category related to butyric acid metabolism identified by PICRUSt prediction of functional profiling of the microbial communities based on the 16S rRNA gene sequences. P value of box plots indicate the result of Kruskal-Wallis H-test. Extended error bar plots to the right indicate pairwise comparison among groups with p value * $p<0.05$ (pairwise comparison using Tukey-Kramer post-hoc test).

Figure 7. **Mucosa-associated microbiome of ex-GF IL-10$^{-/-}$ mice colonized with fecal microbiome from NHE3-deficient mice shows significant reductions in protective taxa**. Proximal and distal colonic segments were resected from IL-10$^{-/-}$ mice that had received FMT from either Rag (NHE3$^{+/+}$) or DKO (NHE3xRag2$^{-/-}$) mice. DNA was extracted from colonic segments and the bacterial 16S DNA sequenced to determine the composition of the mucosa-associated microbiome. Data from the proximal colon, the more affected segment in the IL-10-deficiency model, is presented. **A.** Principal coordinate analysis demonstrating beta diversity (unweighted UNIFRAC) of the mucosal microbiome at sacrifice between IL-10$^{-/-}$ recipients of Rag (NHE3$^{+/+}$, blue) or DKO (NHE3xRag2$^{-/-}$, red) FMT. Larger dots represent males, smaller dots represent females. **B.** Family-level microbiome composition of IL-10$^{-/-}$ recipients of FMT from Rag or DKO mice. **C.** Rarefaction plot depicting alpha diversity (observed OTUs) in ex-GF IL-10$^{-/-}$ mice. **D.** Relative abundance of selected bacterial families in the proximal colonic mucosa of ex-GF IL-10$^{-/-}$ mice that had received FMT from either Rag or DKO donors. * $p<0.05$, ** $p<0.01$, *** $p<0.001$.

Figure 8. **Colonization of GF IL-10$^{-/-}$ mice with fecal microbiome from NHE3$^{-/-}$ donors accelerates the onset and severity of colitis in IL-10$^{-/-}$ mice**. **A.** Representative H&E-stained sections from ex-GF IL-10$^{-/-}$ mice colonized with microbiomes from Rag or DKO (NHE3xRag2$^{-/-}$) mice. **B.** Histological inflammation scores in the proximal and distal colon, the composite total score, and the penetrance of disease calculated by the fraction of animals that had a higher histological inflammation score than the median score of the control (IL-10$^{-/-}$ colonized with Rag microbiome) group. **C.** ELISA analysis lipocalin 2 concentration in fecal samples collected at 2, 5, and 7 weeks post-colonization. P values indicated (Mann-Whitney U-test). **D.** Representative colonoscopy images captured at the 5-week time point, depicting colonic mucosa of ex-GF IL-10$^{-/-}$ mice colonized with microbiomes from either Rag (top panel) or DKO mice (bottom panel). **E.** Immunofluorescence imaging of Ly6B.2^{+}, CD4^{+}, and cleaved caspase 3^{+} cells as seen in proximal and distal colonic sections (200x magnification); quantitation of Ly6B.2^{+}, CD4^{+}, and cleaved caspase 3^{+} cells by colonic segment. For cleaved caspase 3, pixel intensity per field of vision is also calculated (* $p<0.05$).

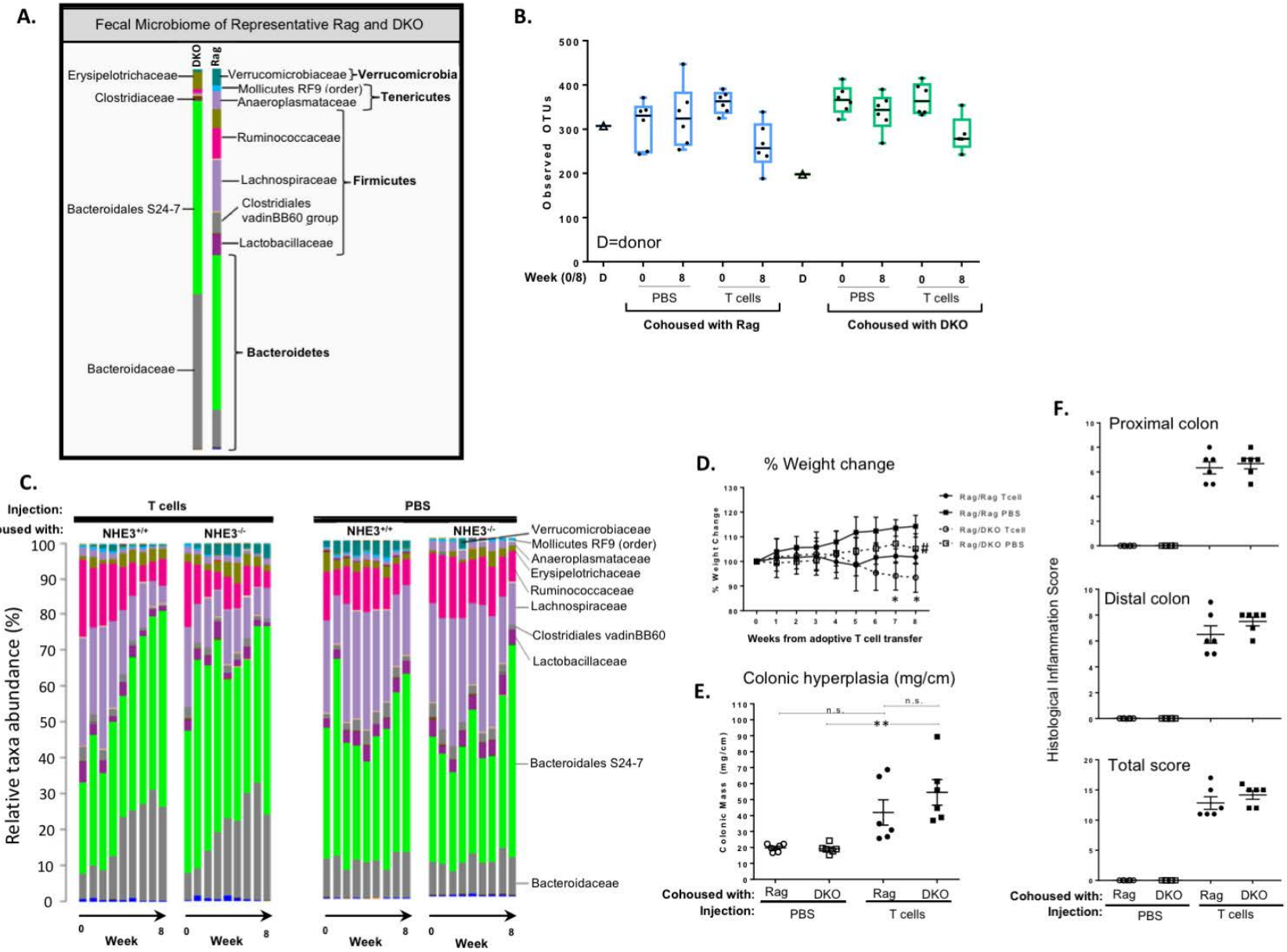
A.
Fecal Microbiome of Representative Rag and DKO
DKO
Rag
Erysipelotrichaceae
Clostridiaceae
Bacteroidales S24-7
Bacteroidaceae
Verrucomicrobiaceae
Mollicutes RF9 (order)
Anaeroplasmataceae
Ruminococcaceae
Lachnospiraceae
Clostridiales vadinBB60 group
Lactobacillaceae
Verrucomicrobia
Tenericutes
Firmicutes
Bacteroidetes
B.
Observed OTUs
D=donor
Week (0/8)
PBS
T cells
Cohoused with Rag
Cohoused with DKO
C.
Injection:
Cohoused with:
T cells
PBS
NHE3+/+
NHE3-/-
Relative taxa abundance (%)
Week
Verrucomicrobiaceae
Mollicutes RF9 (order)
Anaeroplasmataceae
Erysipelotrichaceae
Ruminococcaceae
Lachnospiraceae
Clostridiales vadinBB60
Lactobacillaceae
Bacteroidales S24-7
Bacteroidaceae
D.
% Weight change
% Weight Change
Weeks from adoptive T cell transfer
Rag/Rag Tcell
Rag/Rag PBS
Rag/DKO Tcell
Rag/DKO PBS
E.
Colonic hyperplasia (mg/cm)
Colonic Mass (mg/cm)
n.s.
**
Cohoused with:
Injection:
Rag
DKO
PBS
T cells
F.
Proximal colon
Distal colon
Total score
Histological Inflammation Score

Figure 1

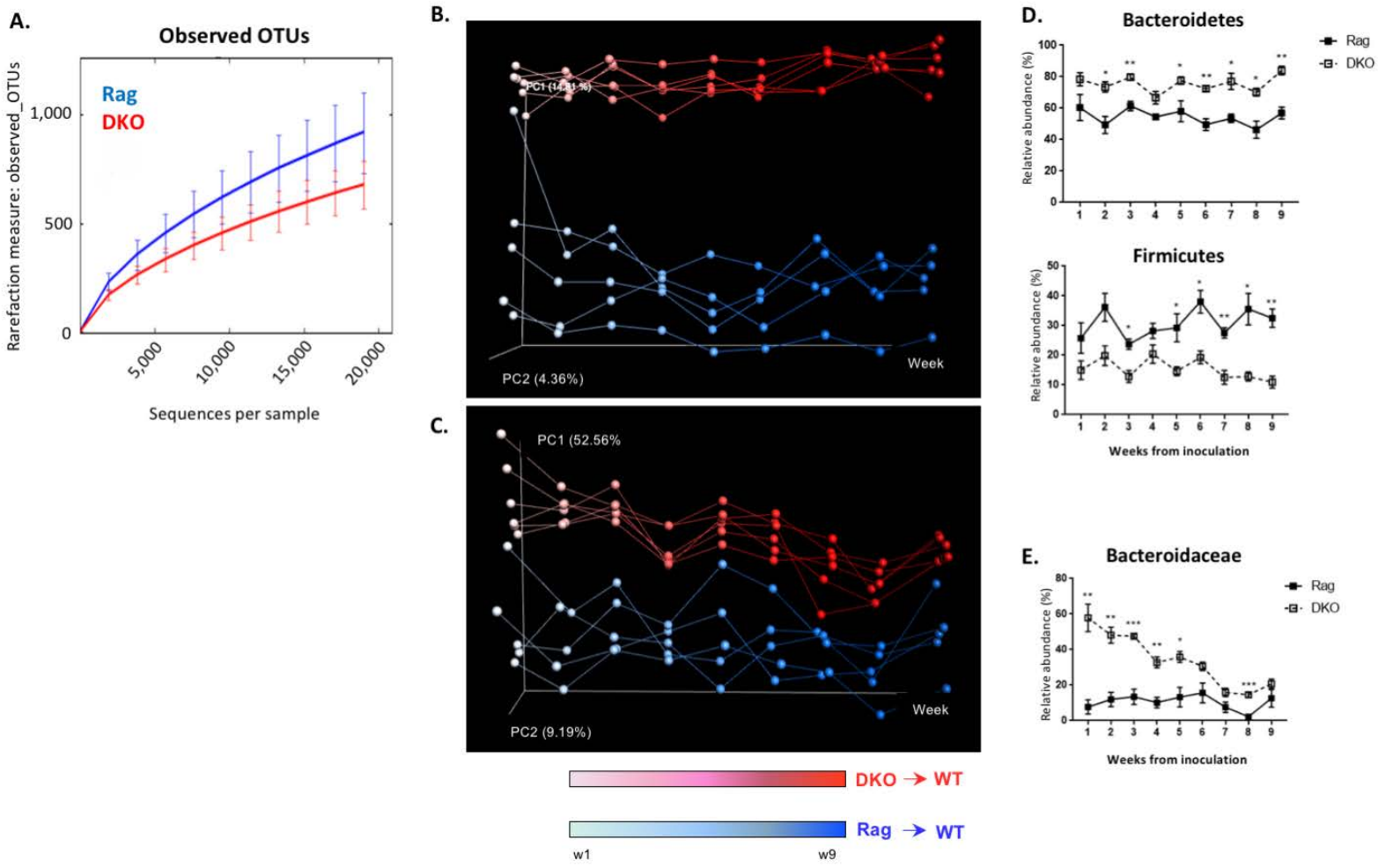
A.
Observed OTUs
Rag
DKO
Rarefaction measure: observed_OTUs
1,000
500
0
5,000
10,000
15,000
20,000
Sequences per sample
B.
PC1 (14.31%)
PC2 (4.36%)
Week
C.
PC1 (52.56%
PC2 (9.19%)
Week
DKO → WT
Rag → WT
w1
w9
D.
Bacteroidetes
Rag
DKO
Relative abundance (%)
Firmicutes
Relative abundance (%)
Weeks from inoculation
E.
Bacteroidaceae
Rag
DKO
Relative abundance (%)
Weeks from inoculation

Figure 2

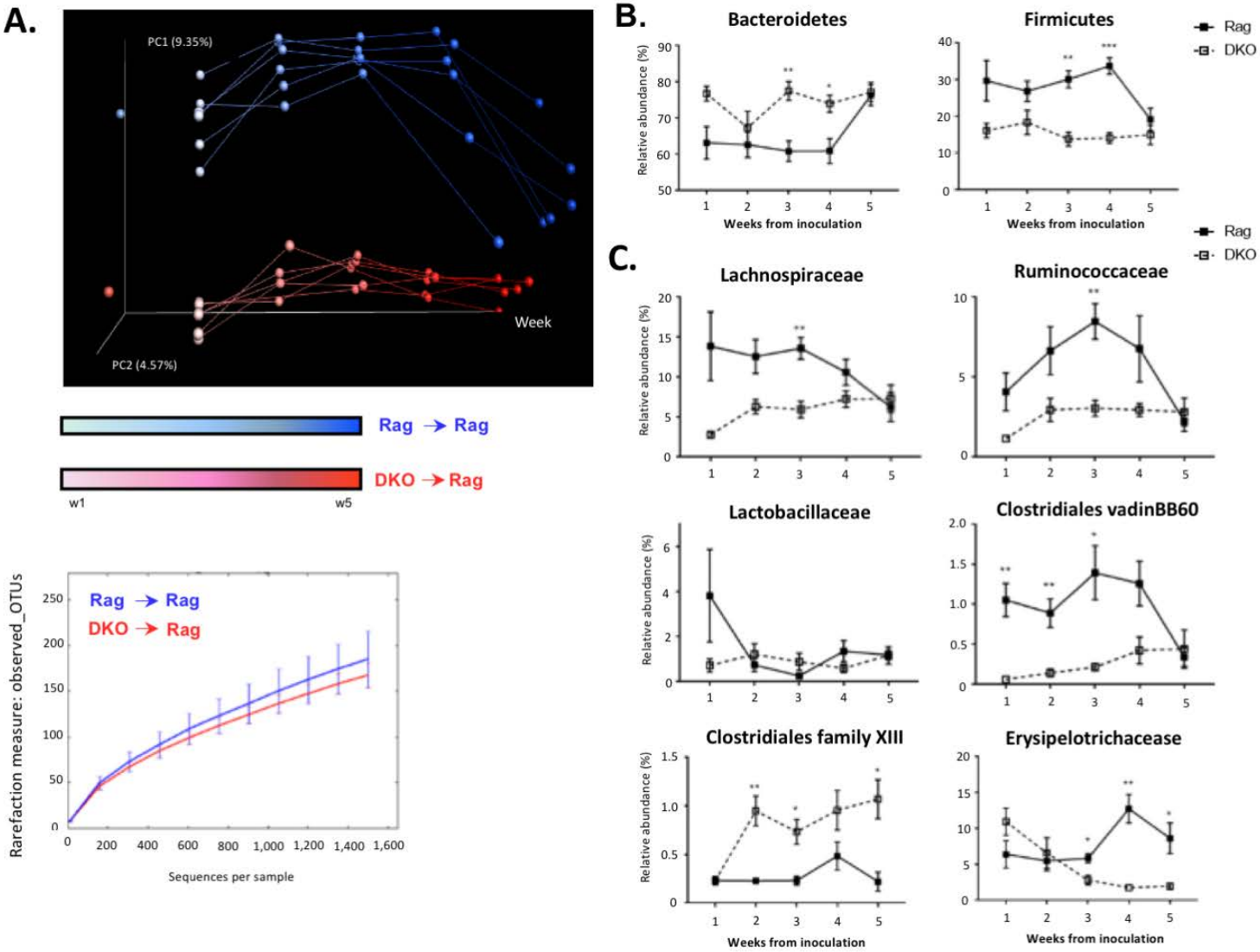
A.
PC1 (9.35%)
PC2 (4.57%)
Week
Rag → Rag
DKO → Rag
w1
w5
Rarefaction measure: observed_OTUs
Sequences per sample
B.
Bacteroidetes
Firmicutes
Relative abundance (%)
Weeks from inoculation
Rag
DKO
C.
Lachnospiraceae
Ruminococcaceae
Lactobacillaceae
Clostridiales vadinBB60
Clostridiales family XIII
Erysipelotrichacease

Figure 3

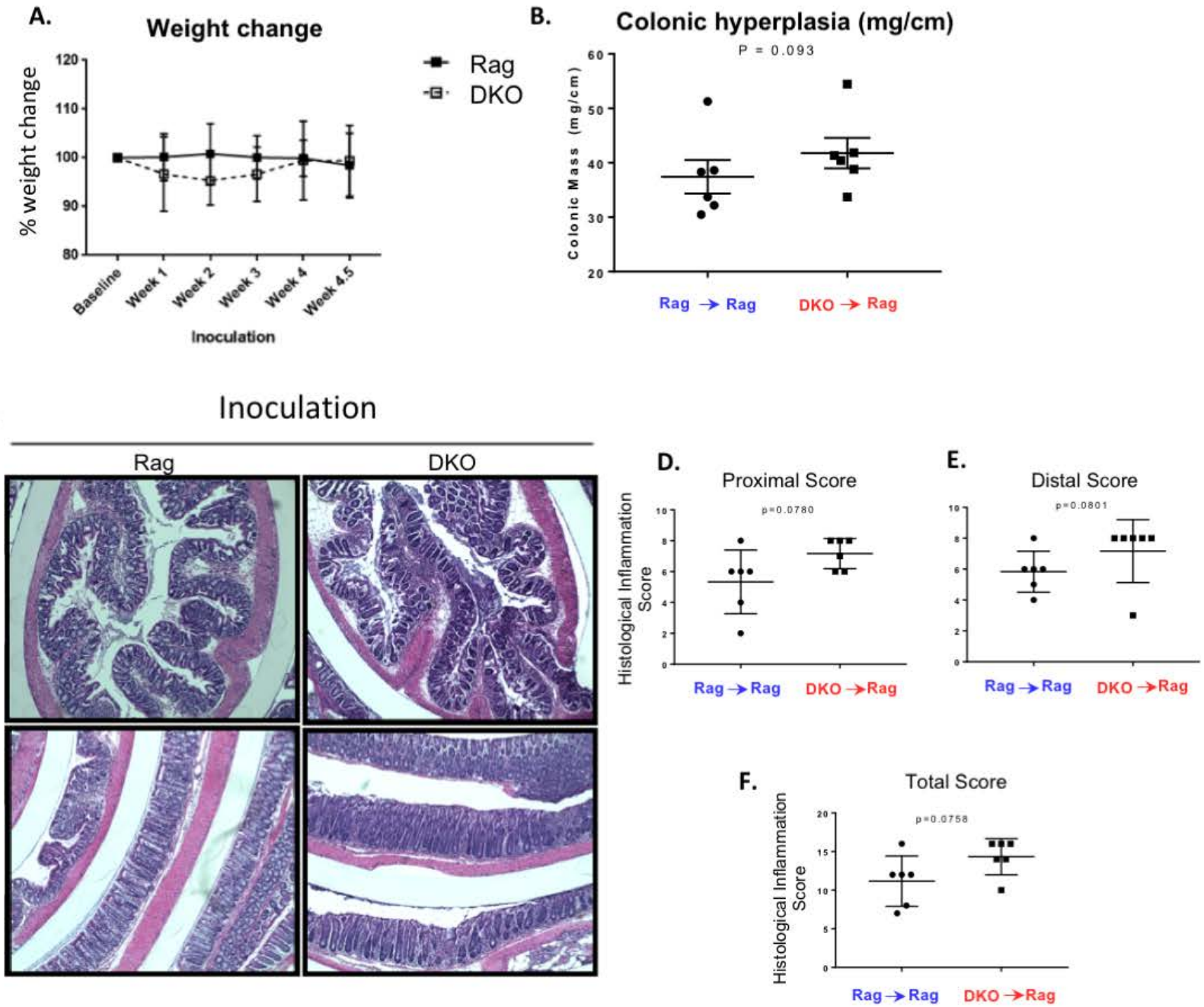
A.
Weight change
% weight change
120
110
100
90
80
Baseline
Week 1
Week 2
Week 3
Week 4
Week 4.5
Inoculation
Rag
DKO
B.
Colonic hyperplasia (mg/cm)
P = 0.093
Colonic Mass (mg/cm)
60
50
40
30
20
Rag → Rag
DKO → Rag
C.
Inoculation
Rag
DKO
Proximal Colon
Distal Colon
D.
Proximal Score
p=0.0780
Histological Inflammation Score
Rag → Rag
DKO → Rag
E.
Distal Score
p=0.0801
Rag → Rag
DKO → Rag
F.
Total Score
p=0.0758
Histological Inflammation Score
20
15
10
5
0
Rag → Rag
DKO → Rag

Figure 4

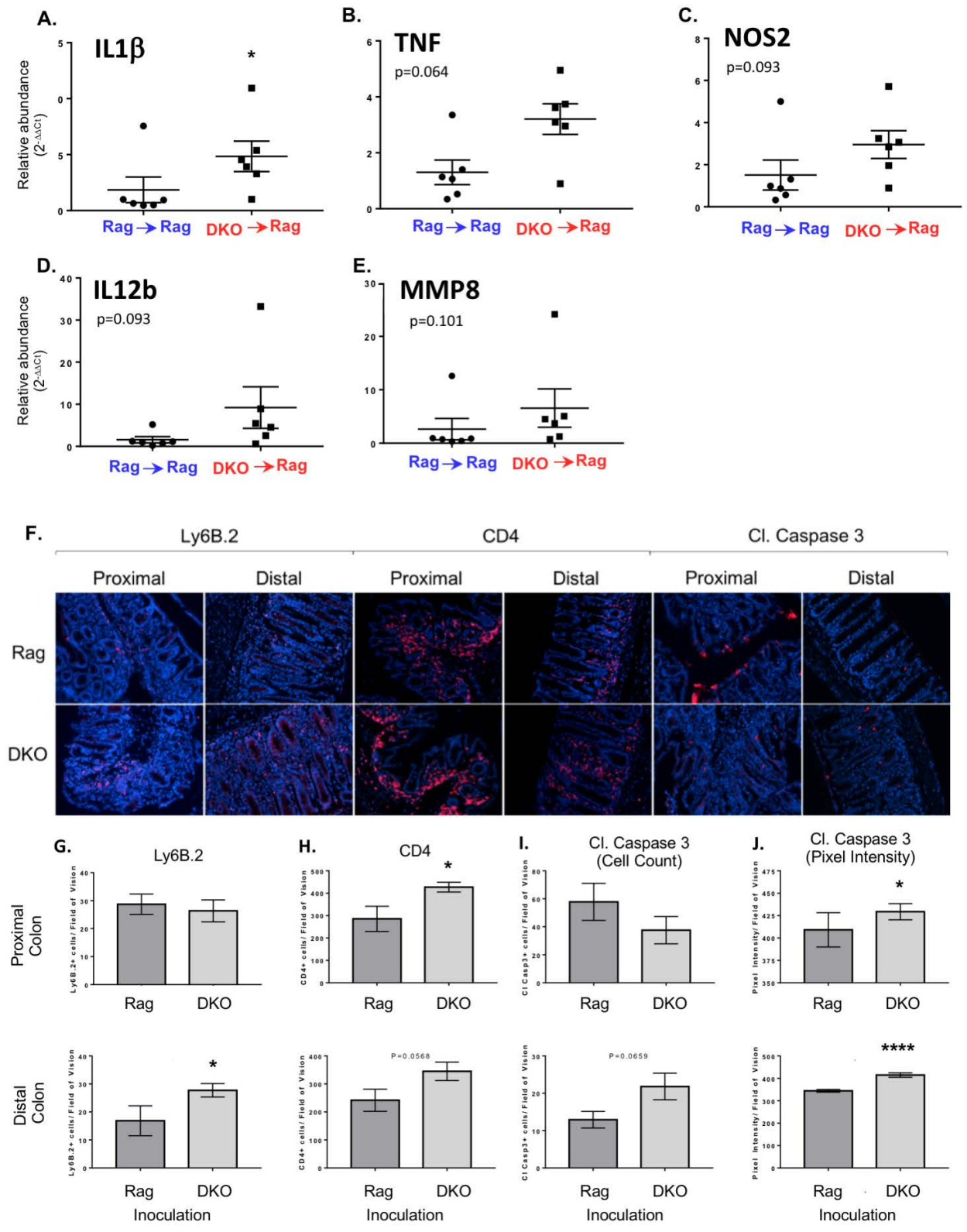
A.
IL1β
Relative abundance (2-ΔΔCt)
*
Rag → Rag
DKO → Rag
B.
TNF
p=0.064
C.
NOS2
p=0.093
D.
IL12b
p=0.093
E.
MMP8
p=0.101
F.
Ly6B.2
CD4
Cl. Caspase 3
Proximal
Distal
Rag
DKO
G.
Ly6B.2
H.
CD4
I.
Cl. Caspase 3 (Cell Count)
J.
Cl. Caspase 3 (Pixel Intensity)
Proximal Colon
Distal Colon
P=0.0568
P=0.0659
****
Inoculation

Figure 5

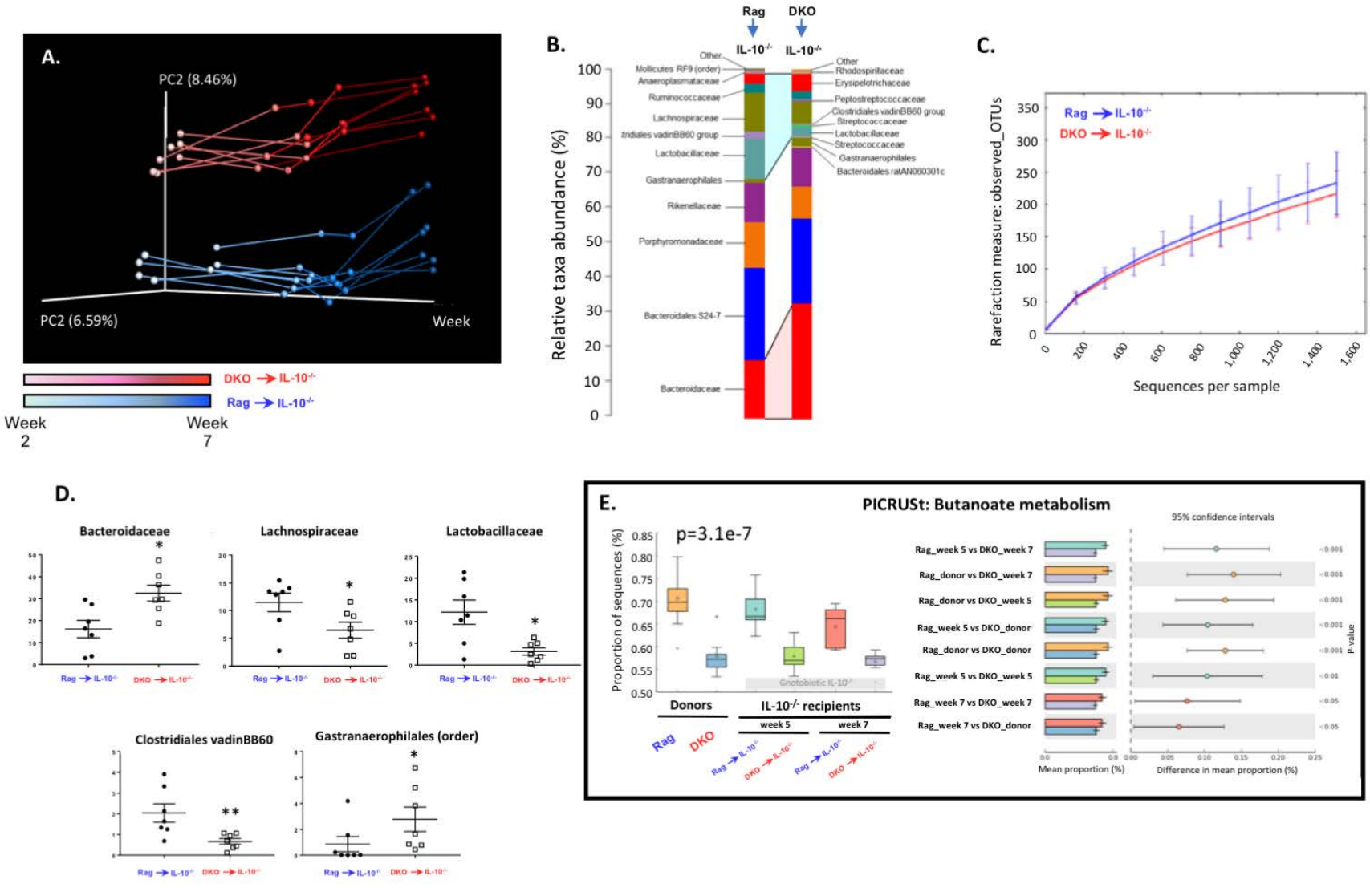
A.
PC2 (8.46%)
PC2 (6.59%)
Week
DKO → IL-10-/-
Rag → IL-10-/-
Week 2
Week 7
B.
Rag
DKO
IL-10-/-
IL-10-/-
Relative taxa abundance (%)
Other
Mollicutes RF9 (order)
Anaeroplasmataceae
Ruminococcaceae
Lachnospiraceae
Clostridiales vadinBB60 group
Lactobacillaceae
Gastranaerophilales
Rikenellaceae
Porphyromonadaceae
Bacteroidales S24-7
Bacteroidaceae
Other
Rhodospirillaceae
Erysipelotrichaceae
Peptostreptococcaceae
Clostridiales vadinBB60 group
Streptococcaceae
Lactobacillaceae
Streptococcaceae
Gastranaerophilales
Bacteroidales ratAN060301c
C.
Rarefaction measure: observed_OTUs
Rag → IL-10-/-
DKO → IL-10-/-
Sequences per sample
D.
Relative abundance (%)
Bacteroidaceae
Lachnospiraceae
Lactobacillaceae
Clostridiales vadinBB60
Gastranaerophilales (order)
E.
PICRUSt: Butanoate metabolism
p=3.1e-7
Proportion of sequences (%)
Donors
IL-10-/- recipients
week 5
week 7
Rag
DKO
95% confidence intervals
Rag_week 5 vs DKO_week 7
Rag_donor vs DKO_week 7
Rag_donor vs DKO_week 5
Rag_week 5 vs DKO_donor
Rag_donor vs DKO_donor
Rag_week 5 vs DKO_week 5
Rag_week 7 vs DKO_week 7
Rag_week 7 vs DKO_donor
P-value
Mean proportion (%)
Difference in mean proportion (%)

Figure 6

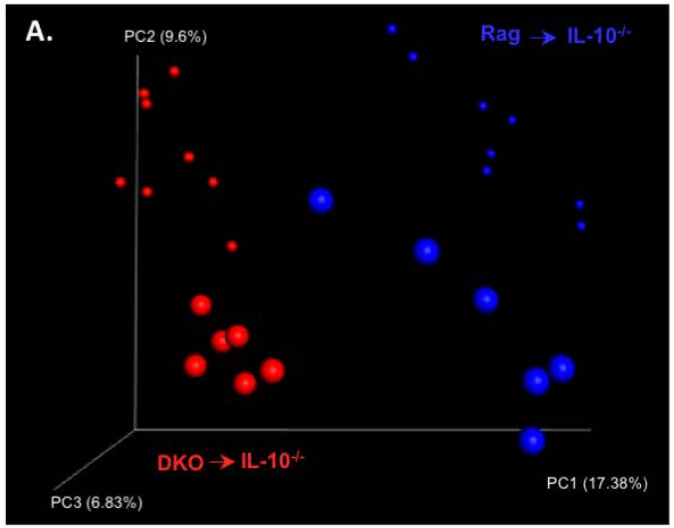
A.
PC2 (9.6%)
Rag → IL-10-/-
DKO → IL-10-/-
PC3 (6.83%)
PC1 (17.38%)

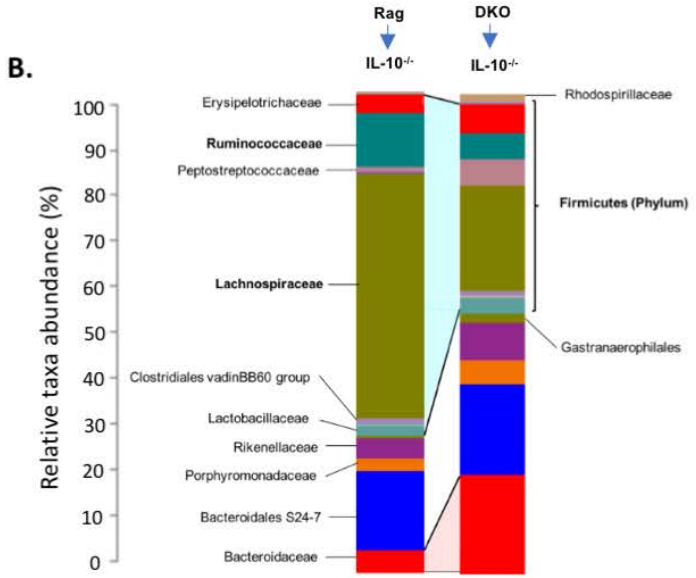
B.
Rag
IL-10-/-
DKO
IL-10-/-
Relative taxa abundance (%)
Erysipelotrichaceae
Ruminococcaceae
Peptostreptococcaceae
Lachnospiraceae
Clostridiales vadinBB60 group
Lactobacillaceae
Rikenellaceae
Porphyromonadaceae
Bacteroidales S24-7
Bacteroidaceae
Rhodospirillaceae
Firmicutes (Phylum)
Gastranaerophilales

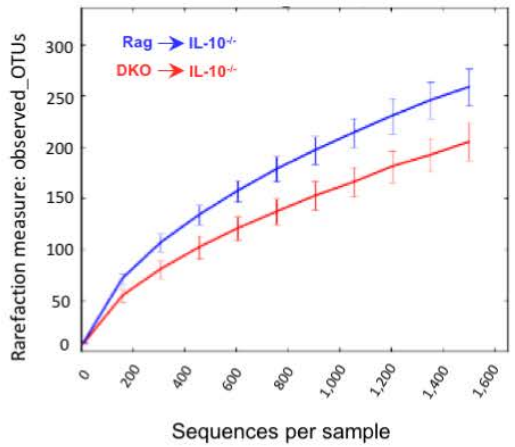
C.
Rag → IL-10-/-
DKO → IL-10-/-
Rarefaction measure: observed_OTUs
Sequences per sample

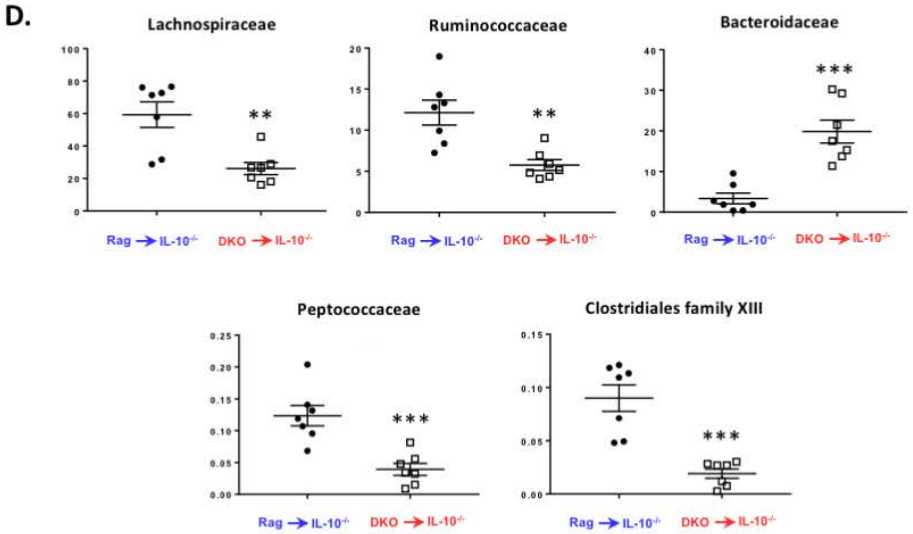
D.
Lachnospiraceae
Ruminococcaceae
Bacteroidaceae
Peptococcaceae
Clostridiales family XIII
Rag → IL-10-/-
DKO → IL-10-/-

Figure 7

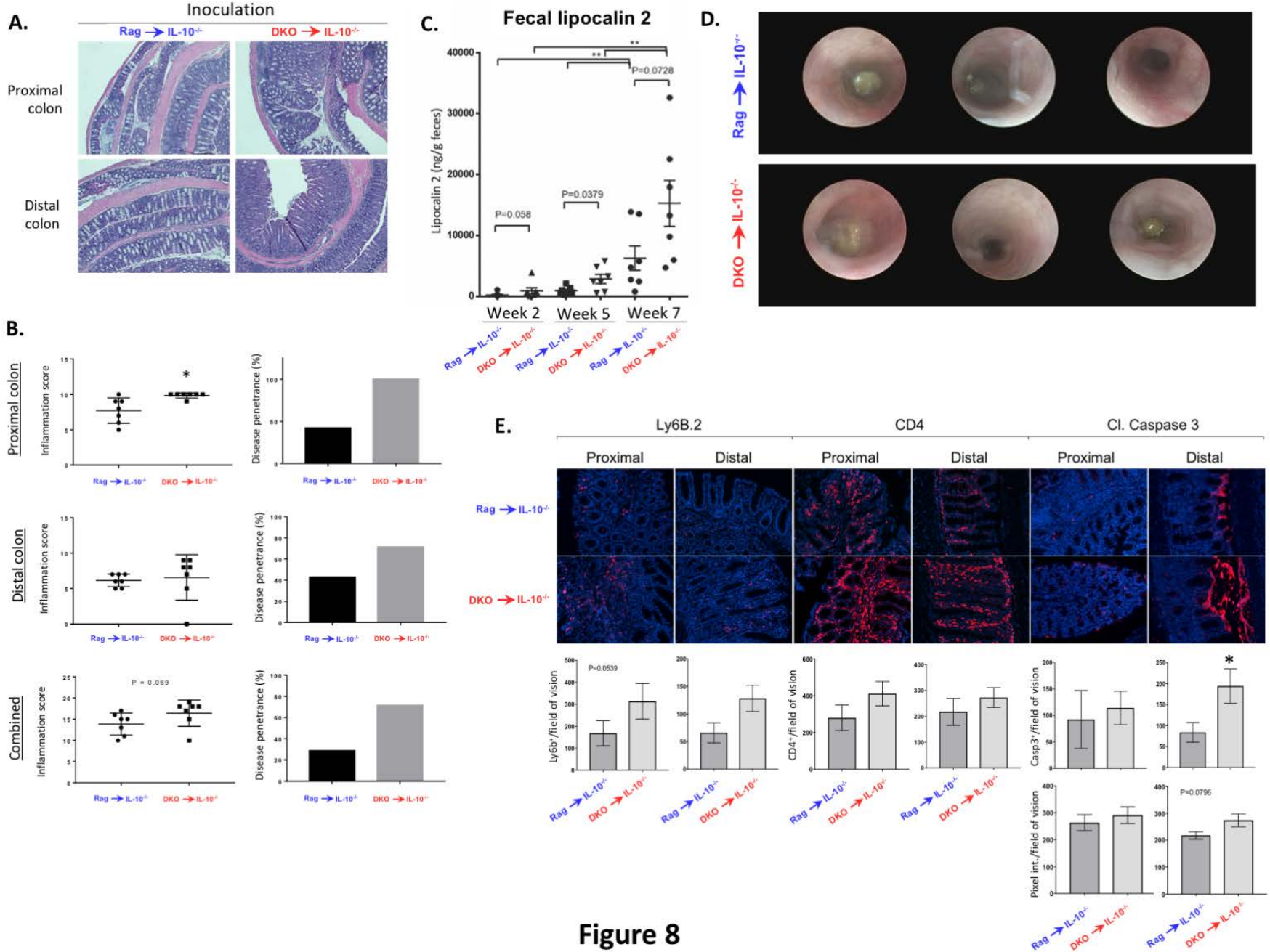
A.
Inoculation
Rag → IL-10-/-
DKO → IL-10-/-
Proximal colon
Distal colon
B.
Proximal colon
Distal colon
Combined
Inflammation score
Disease penetrance (%)
P = 0.069
C.
Fecal lipocalin 2
Lipocalin 2 (ng/g feces)
P=0.058
P=0.0379
P=0.0728
Week 2
Week 5
Week 7
D.
E.
Ly6B.2
CD4
Cl. Caspase 3
Proximal
Distal
Ly6b+/field of vision
CD4+/field of vision
Casp3+/field of vision
Pixel int./field of vision
P=0.0539
P=0.0796

Figure 8

SUPPLEMENTAL DATA: Supplemental Methods

Histology and Pathological Interpretation

Histological preparations were done by the University of Arizona University Animal Care (UAC) Pathology Services core. Colons were resected, gently flushed with PBS to clear debris, and opened lengthwise on nitrocellulose membrane (Millipore, cat #HAWP00010). Longitudinal proximal and distal colonic segments were collected and fixed in 10% buffered formalin phosphate (Fisher Chemical) overnight at 4°C. Tissues were subsequently transferred from formalin into 70% ethanol and submitted to UAC for embedding in paraffin. Blocks were cut into 5μm thick sections, mounted on slides, and stained with hematoxylin and eosin (H&E). Pathological interpretation and inflammation scoring was performed by an experienced veterinary pathologist (D. Besselsen; UAC) blinded to the experimental design and sample group assignment. Briefly, sections were scored in point-based fashion on four different parameters: mucosal hyperplasia (0-3, in reference to mucosal thickness), extent of inflammation or proliferation (0-3, based on the percentage of segment affected), inflammation (0-4, in reference to whether inflammation is limited to the mucosa or has extended deeper into the submucosa, and whether there are erosions, loss of structure, ulcerations or abscesses), and extent of dysplasia (0-3, in reference to the percentage of the segment with dysplasia). Since our models have not been precancerous, the highest score for an individual segment is 10. Proximal and distal colonic segments were scored separately, and summed together for a total score.

Adoptive T Cell Transfer

Adoptive transfer of naïve $CD4^+CD45RB^{HI}$ T cells was carried out as described and previously performed.[1] Briefly, spleens were resected from wild-type 129SvEv mice and collected into complete medium (RPMI + GlutaMAX, Gibco) containing 10% fetal bovine serum (FBS, HyClone), 5% penicillin streptomycin (HyClone), and 5% non-essential amino acids (NEAA, HyClone). Splenocytes were gently released from the tissue through the mechanical mashing of the tissue against a 100μm cell strainer (Alkali Scientific, Inc.) in medium, using the blunt end of a 1ml syringe plunger (BD). Following red cell lysis (Pharm Lyse, BD), released splenocytes were enriched for CD4 expression using an anti-biotin negative selection kit and run through LS columns (Miltenyi Biotec, kit cat# 130-095-248, column cat# 130-042-401). CD4-enriched splenocytes were fluorescently labeled with PE-conjugated rat anti-mouse CD4 and FITC-conjugated rat anti-mouse CD45RB antibodies (BD, cat#'s 553059 and 553100 respectively), and sorted on the FACSAria III (BD Biosciences, San Jose, CA) operated by the University of Arizona Flow Cytometry Core Facility for $CD4^+$ and the top 40% of CD45RB-expressing cells. Sorted cells were counted and injected intraperitoneally (i.p.) at $5x10^5$ cells/ml in 500μl sterile PBS. Control animals were injected with 500μl sterile PBS. Animals were monitored weekly for weight change and stool collection.

Mucosal DNA and RNA extraction

Mucosal DNA and RNA were isolated from colonic segments using the AllPrep DNA/RNA Mini Kit (Qiagen, cat # 80204) with a modified protocol. Colons were resected from mice, flushed with PBS, and opened lengthwise on nitrocellulose membrane. Lengthwise segments of the proximal and distal colons were taken separately, snap frozen in liquid nitrogen, and stored at -80°C. Upon processing, tissues were kept frozen

until the moment they were added to 2ml tubes containing 0.5mm glass beads (Fisherbrand, cat # 15-340-152) with pre-added Buffer RLT Plus (Qiagen), with 1% β-mercaptoethanol (β-ME, GeneMate) and 0.5% Reagent DX (Qiagen, cat # 19088). Samples were homogenized by bead-beating with TissueLyser II (Qiagen, formerly MoBio) at a frequency of 20 Hz for 5 minutes before flipping the orientation and repeating for another 5 minutes. Following bead-beating, we proceeded with the kit protocol instructions. Extracted DNA and RNA were stored at -80°C until analyzed.

Next-Generation Sequencing

The V4 fragments of 16S rRNA gene from extracted fecal and mucosal DNA were sequenced using an Illumina MiSeq platform. Briefly, a library was created by the amplification of the V4 fragment of bacterial 16S rRNA gene by polymerase chain reaction (PCR) using 515F and 806R primers with a unique barcoded sequence for each sample[25] and 5 Prime Hot Mastermix (5 Prime, Germany). Amplification was verified by running on an agarose gel and amplicons were quantified using Picogreen (Invitrogen) per manufacturer instructions. 240ng of DNA from each sample were pooled and 500ul the pooled library was run on an agarose gel. To remove primer dimers and/or non-specific PCR products the ~400bp band was extracted from the gel using UltraClean DNA Purification Kit (MoBio) followed by UltraClean PCR Clean-Up Kit (MoBio). Pooled and purified library was quantified by qPCR with the KAPA Library Quantification Kit (KAPA Biosystems). Due to low diversity of the library, 5% of control PhiX library (Illumina) was added and the final concentration of 7pM was paired ended sequenced in-house on the

Illumina MiSeq (MiSeq Control Software version 2.5.0), using custom primers[2] and the MiSeq Illumina Sequencing Kit V2 2x150bp kit (Illumina).

Bioinformatic Analysis of the Microbiome

Bioinformatic analysis of sequenced amplicons was performed using the QIIME 1.9.1 software package,[3] a Python-based, open-source command-line package developed for the analysis of microbial datasets. Microbial sequences were demultiplexed and assigned to operational taxonomic units (OTUs) by an open-reference OTU picking algorithm[4] based on comparison to the SILVA reference database (release 128, https://www.arb-silva.de)[5] at a similarity level of 97%. Unassigned sequences were subsequently clustered *de novo*. Quality filtering was unique to each experiment, based on the number of sequences per sample. Filtering cutoffs were assigned to exclude any samples with dramatically decreased sequence counts from the majority, or at minimum any samples with less than 1000 sequences per sample. On average between one and five samples were excluded per experiment. Relative abundance of taxa and core diversity (including both alpha and beta diversity metrics) were calculated for each experiment, from which principal coordinate (PCoA) analyses were generated. For fecal samples, PCoA plots represent beta diversity over time, and for mucosal samples, at the final time point. Unless otherwise indicated, taxonomic analyses in this paper focused on family-level differences at the final experimental time point. Raw data on bacterial abundance at the final time points were transferred into GraphPad Prism version 7.00 for comparisons of individual taxa between groups. For relative abundance of taxa over time, taxa were selected for presentation based on a combination of percent abundance in the

microbiota, statistical difference between groups, known biological relevance, and/or change over time. Individual time points were analyzed in Prism using an unpaired Student T test for each time point.

In order to gain insight into a metabolic potential of the gut microbiome PICRUSt v. 1.1.1 (Phylogenetic Investigation of Communities by Reconstruction of Unobserved States) [6] was used to predict metagenome functional content based on the marker gene, 16S rRNA gene surveys. Briefly, all sequences were searched against the GreenGenes reference database (v. gg_13_8) using *pick_closed_reference_otus.py* script (QIIME 1.9.1),[3] which combines uclust,[4] PyNAST,[7] and FastTree.[8] The command builds a .biom table with OTUs assigned at the 97% identity. Then all samples with less than 2 reads were filtered out. The OTU table was normalized by dividing each OTU by known or predicted number of copies abundance of 16S rRNA gene followed by the creation of the metagenome functional prediction collapsed into the KEGG Pathway categories. Functional prediction data were analyzed and visualized with the Statistical Analysis of Metagenomic profiles (STAMP) software package (release v. 2.1.3),[9] and an ANOVA test was followed by Tukey-Kramer post-hoc test with Bonferroni multiple test correction, or two-sided Welch's t-test with Storey FDR multiple testing correction, was used as appropriate.

Fecal Lipocalin 2 ELISA

Fecal pellets were collected from ex-germ-free IL-10$^{-/-}$ mice and stored at -80°C until use. Fecal suspensions were prepared from frozen fecal samples by recording the weight of each sample, suspending in 1 ml PBS containing 0.1% Tween 20, mixing and

vortexing for 20 minutes at max speed (Vortemp 56, Labnet International), centrifuging at 12,000 rpm, 4°C for 10 min, and collecting the supernatant. Fecal suspensions were stored at -20°C, and used within a couple weeks of preparation. Lipocalin 2 was detected by ELISA (DuoSet, cat# DY1857, ancillary kit cat# DY008; R&D Systems, Bio-Techne Corporation, Minneapolis, MN), with sample dilutions of 1:100, 1:500, and 1:1000. Quantification of protein was detected by measure optical density against a standard curve, according to kit specifications, and measured by SpectraMax M3 (Molecular Devices).

Immunofluorescence and Cell Quantitation

Parrafin embedded colonic segments were sliced and mounted on slides. Cuts were subsequently heated to 60°C for 3-5 minutes to melt paraffin, and taken through a series of baths in xylenes, progressively more hydrous ethanol, and water. Antigen retrieval was performed by boiling in citrate buffer for 10 minutes and allowing to cool to room temperature for 45-60 minutes. Slides were blocked in PBS + 1% BSA, with 2-10% serum from the animal used in the secondary antibody. They were incubated in primary antibody overnight at 4°C in a humidified container in the dark, washed 3x in PBS + 1% BSA, and incubated in secondary antibody for one hour at room temperature in the dark. Finally, slides were washed three more times in PBS + 1% BSA, including one wash with 1:10,000 DAPI, coverslipped, allowed to dry overnight, and imaged. Slides were imaged within several days of staining.

References for Supplemental Methods

1. Laubitz D, Harrison CA, Midura-Kiela MT, Ramalingam R, Larmonier CB, Chase JH *et al.* Reduced Epithelial Na+/H+ Exchange Drives Gut Microbial Dysbiosis and Promotes Inflammatory Response in T Cell-Mediated Murine Colitis. *PLoS One* 2016; **11**(4)**:** e0152044.

2. Caporaso JG, Lauber CL, Walters WA, Berg-Lyons D, Huntley J, Fierer N *et al.* Ultra-high-throughput microbial community analysis on the Illumina HiSeq and MiSeq platforms. *ISME J* 2012; **6**(8)**:** 1621-1624.

3. Caporaso JG, Kuczynski J, Stombaugh J, Bittinger K, Bushman FD, Costello EK *et al.* QIIME allows analysis of high-throughput community sequencing data. *Nat Methods* 2010; **7**(5)**:** 335-336.

4. Edgar RC. Search and clustering orders of magnitude faster than BLAST. *Bioinformatics* 2010; **26**(19)**:** 2460-2461.

5. Quast C, Pruesse E, Yilmaz P, Gerken J, Schweer T, Yarza P *et al.* The SILVA ribosomal RNA gene database project: improved data processing and web-based tools. *Nucleic Acids Res* 2013; **41**(Database issue)**:** D590-596.

6. Langille MG, Zaneveld J, Caporaso JG, McDonald D, Knights D, Reyes JA *et al.* Predictive functional profiling of microbial communities using 16S rRNA marker gene sequences. *Nat Biotechnol* 2013; **31**(9)**:** 814-821.

7. Caporaso JG, Bittinger K, Bushman FD, DeSantis TZ, Andersen GL, Knight R. PyNAST: a flexible tool for aligning sequences to a template alignment. *Bioinformatics* 2010; **26**(2)**:** 266-267.

8. Price MN, Dehal PS, Arkin AP. FastTree 2--approximately maximum-likelihood trees for large alignments. *PLoS One* 2010; **5**(3)**:** e9490.

9. Parks DH, Tyson GW, Hugenholtz P, Beiko RG. STAMP: statistical analysis of taxonomic and functional profiles. *Bioinformatics* 2014; **30**(21)**:** 3123-3124.

SUPPLEMENTAL DATA: Supplemental Figure Legends

Figure S1. **Figure S1**. **Experimental design for each experiment presented in the paper**. **A**. Rag2$^{-/-}$ (Rag) mice were cohoused in a 2:3 ratio with either Rag or NHE3xRag$^{-/-}$ (DKO) mice for one week prior to injection with naïve CD4^{+}CD45RB^{hi} T cells, or control injection with PBS. Animals were maintained for eight weeks with weekly stool collection before sacrifice and tissue collection. **B**. Fecal pellets were pooled from Rag mice and, separately, DKO mice to make donor slurries. The same two pools of Rag and DKO donors were used for B, C, and D for consistency. Fecal slurries were used to orally inoculate germ-free wildtype mice. Animals were monitored for nine weeks with weekly stool collection before sacrifice. **C**. Rag or DKO stool was pooled to make fecal slurries that was orally inoculated into germ-free Rag1$^{-/-}$ mice, followed by adoptive transfer of naïve CD4^{+}CD45RB^{hi} T cells. Animals were maintained for five weeks with weekly stool collection before sacrifice at the recommendation of facility veterinary personnel, at which time tissues were also collected. **D**. Rag or DKO stool was pooled to make fecal slurries that were orally inoculated into germ-free Il-10$^{-/-}$ mice. Animals were maintained for seven weeks with regular stool collection before sacrifice and subsequent tissue collection.

Figure S2. **Taxonomic shifts in the microbiome of T-cell transferred Rag mice in co-housing.** Relative abundance of selected taxa at weekly time points. Nearly identical patterns were observed regardless of the co-housed donors (Rag or DKO). For clarity, only PBS-injected (blue) or T-cell transferred (black) Rag mice co-housed with Rag (NHE3-sufficient) mice are shown. * $p<0.05$, ** $p<0.01$, *** $p<0.001$, # $p<0.06$, Two-way ANOVA.

Figure S3. **Co-housing with NHE3-deficient DKO mice does not lead to increased mucosal inflammation after adoptive T-cell transfer.** **A**. H&E staining of proximal and distal colon in PBS-treated or T-cell transferred Rag mice co-housed with either Rag or DKO (NHE3xRag) mice (10x magnification) **B**. RT-qPCR depicting colonic expression of selected inflammatory mediators in Rag mice treated and co-housed as described above.

Figure S4. **Most taxonomic groups remain stably transplanted over time following FMT into wildtype recipients**. Fecal microbiome transplant

(FMT) from Rag ($NHE3^{+/+}$) or DKO (NHE3xRag double knockout) mice into wildtype germ-free mice. Mice were maintained for nine weeks post-colonization with weekly fecal collections (w1 to w9). **A**. Family-level microbiome composition from weekly fecal collections in WT GF mice that had received FMT from either Rag or DKO fecal donors. **B**. Relative abundance of selected bacterial families in wildtype FMT recipients. * $p<0.05$, ** $p<0.01$, Two-way ANOVA.

Figure S5. Relative abundance of selected taxa over time in fecal samples of the IL-$10^{-/-}$ recipients of Rag or DKO microbiomes. Germ-free IL-$10^{-/-}$ mice were colonized with fecal microbiome from Rag ($NHE3^{+/+}$) or DKO (NHE3xRag) mice and fecal samples were collected and analyzed prospectively between weeks 2-7 after colonization. * $p<0.05$, ** $p<0.01$, *** $p<0.001$, **** $p<0.0001$. Two-way ANOVA.

Figure S6. PICRUSt prediction of functional profiling of the microbial communities of gnotobiotic IL-$10^{-/-}$ mice at 5 weeks post-colonization based on the 16S rRNA gene sequences. Extended error bar plot indicating differences in functional profiles of the microbiota (at taxonomic Level 3) of gnotobiotic IL-$10^{-/-}$ mice 5 weeks after FMT from Rag of DKO ($NHE3xRag2^{-/-}$) donors. All unclassified reads were removed and categories with minimum of 20 reads, and P value greater than 0.05 is displayed. Categories are sorted by q value calculated using two-sided Welch's t-test with Storey FDR multiple testing correction.

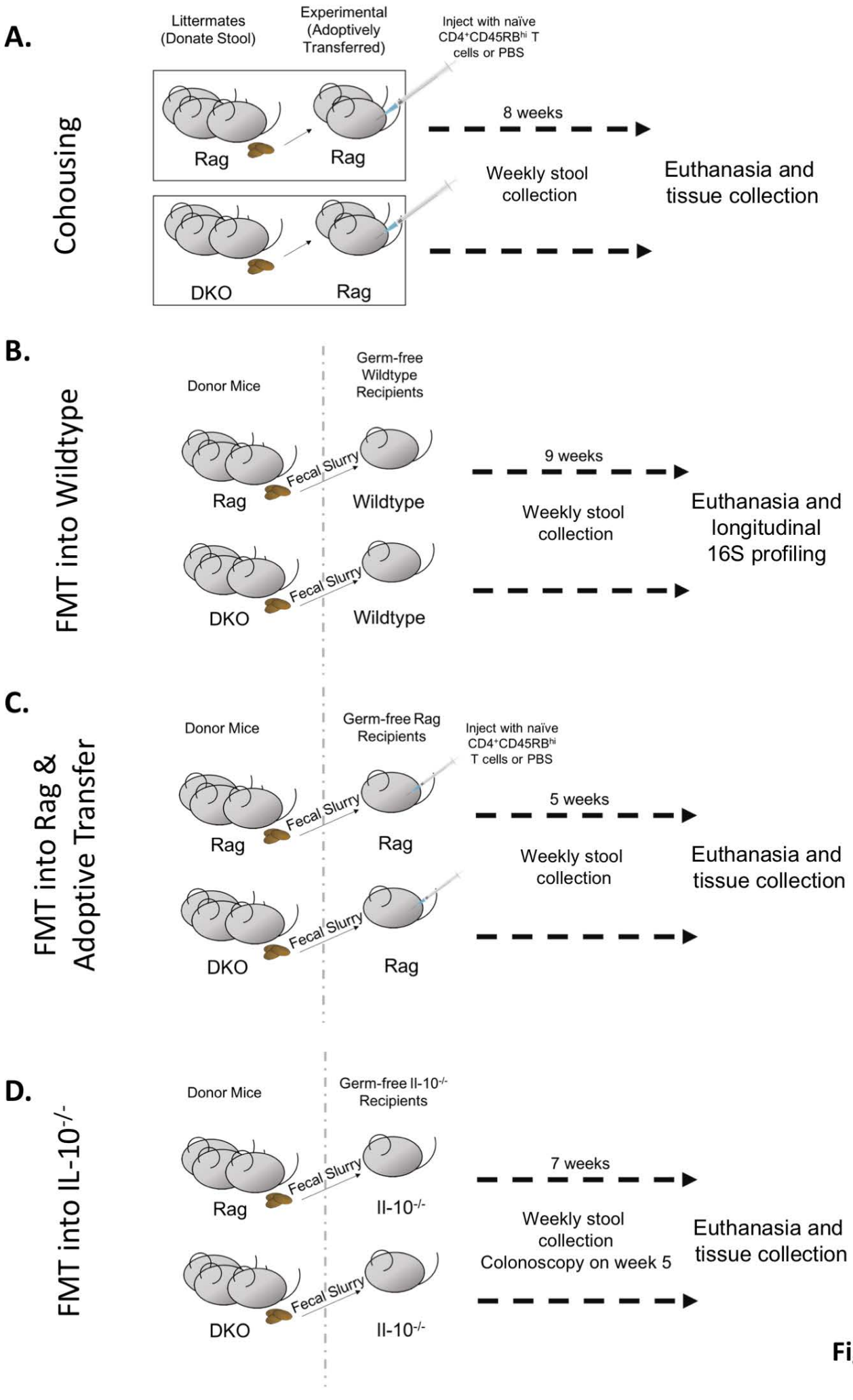
A.
Cohousing
Littermates (Donate Stool)
Experimental (Adoptively Transferred)
Inject with naïve CD4+CD45RBhi T cells or PBS
Rag
Rag
8 weeks
Weekly stool collection
Euthanasia and tissue collection
DKO
Rag
B.
FMT into Wildtype
Donor Mice
Germ-free Wildtype Recipients
Fecal Slurry
Rag
Wildtype
9 weeks
Weekly stool collection
Euthanasia and longitudinal 16S profiling
Fecal Slurry
DKO
Wildtype
C.
FMT into Rag & Adoptive Transfer
Donor Mice
Germ-free Rag Recipients
Inject with naïve CD4+CD45RBhi T cells or PBS
Fecal Slurry
Rag
Rag
5 weeks
Weekly stool collection
Euthanasia and tissue collection
Fecal Slurry
DKO
Rag
D.
FMT into IL-10-/-
Donor Mice
Germ-free Il-10-/- Recipients
Fecal Slurry
Rag
Il-10-/-
7 weeks
Weekly stool collection
Colonoscopy on week 5
Euthanasia and tissue collection
Fecal Slurry
DKO
Il-10-/-

Figure S1

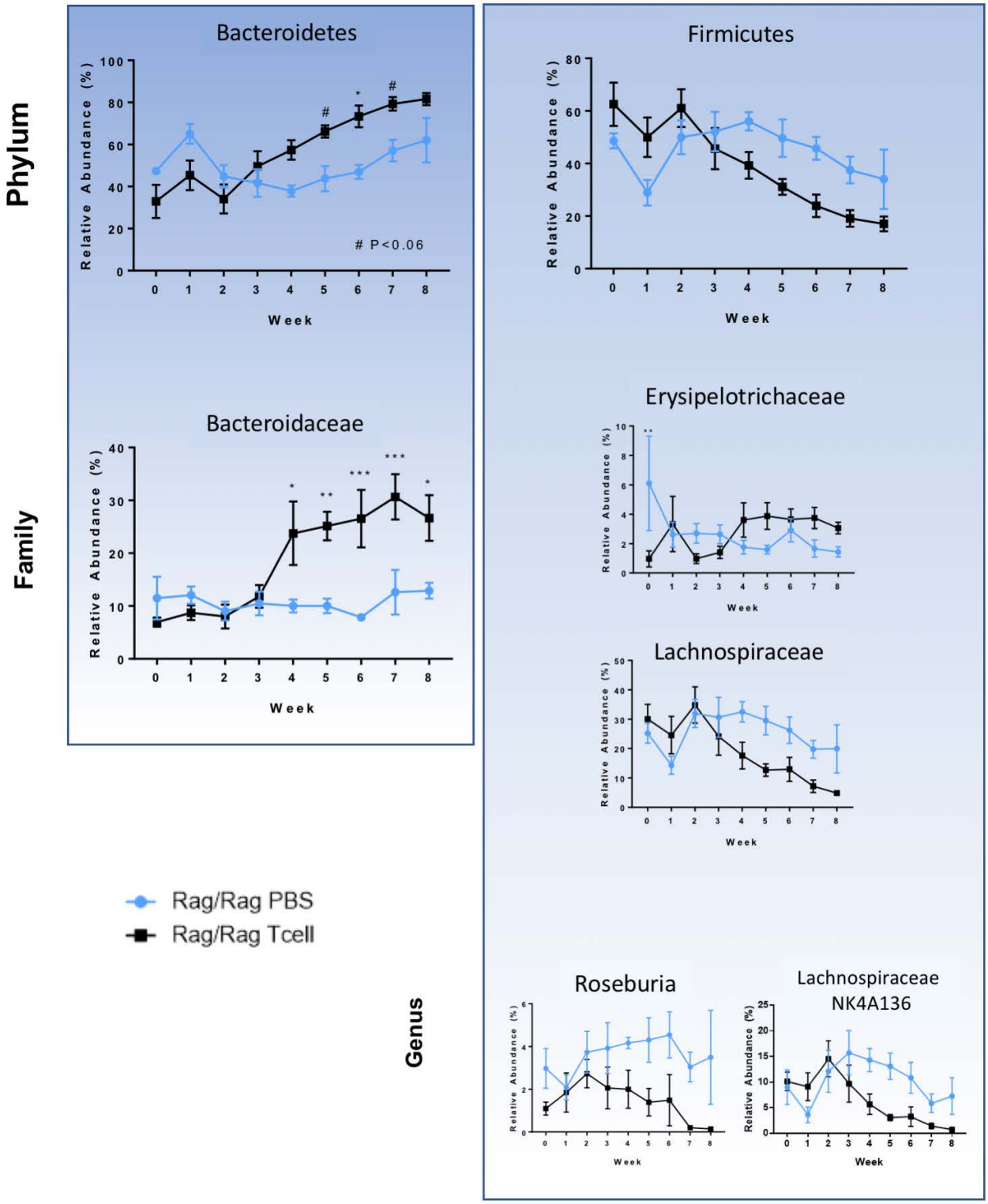
Phylum
Family
Genus
Bacteroidetes
Relative Abundance (%)
Week
# P<0.06
Firmicutes
Bacteroidaceae
Erysipelotrichaceae
Lachnospiraceae
Rag/Rag PBS
Rag/Rag Tcell
Roseburia
Lachnospiraceae NK4A136

Figure S2

A.

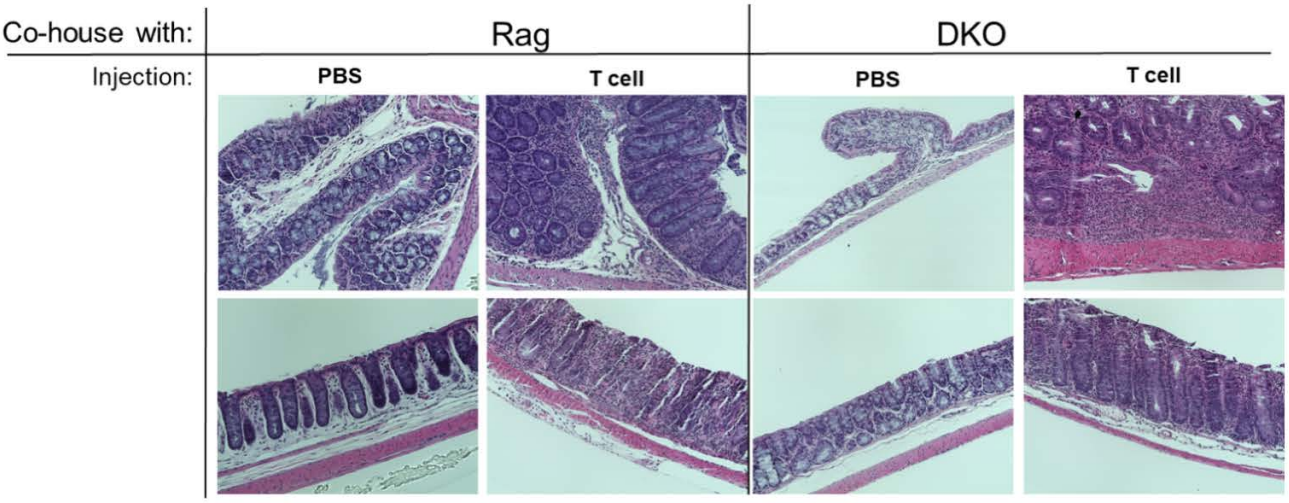
Co-house with:
Rag
DKO
Injection:
PBS
T cell
PBS
T cell

B.

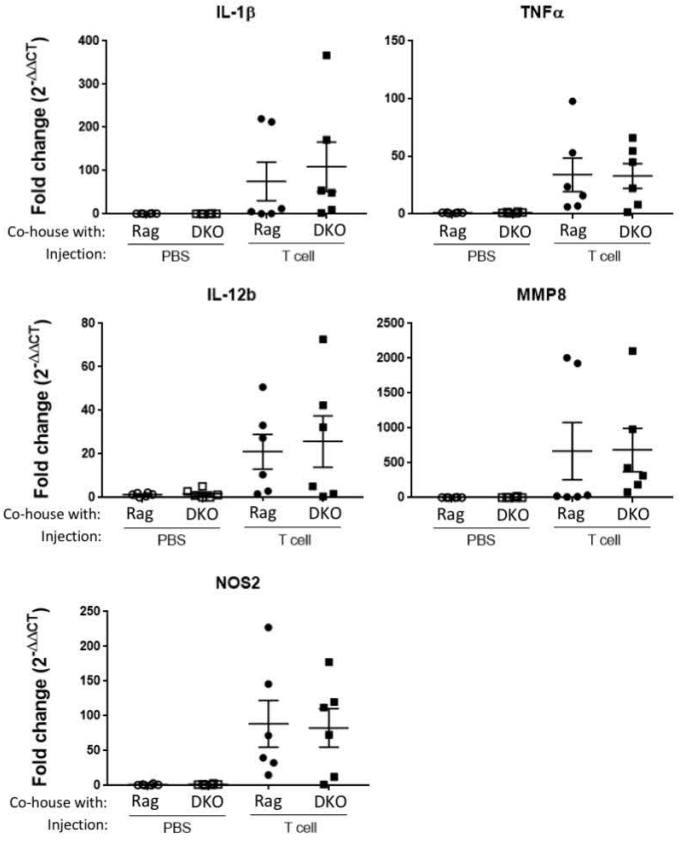
IL-1β
TNFα
IL-12b
MMP8
NOS2
Fold change (2^-ΔΔCT)
Co-house with:
Rag
DKO
Rag
DKO
Injection:
PBS
T cell

Figure S3

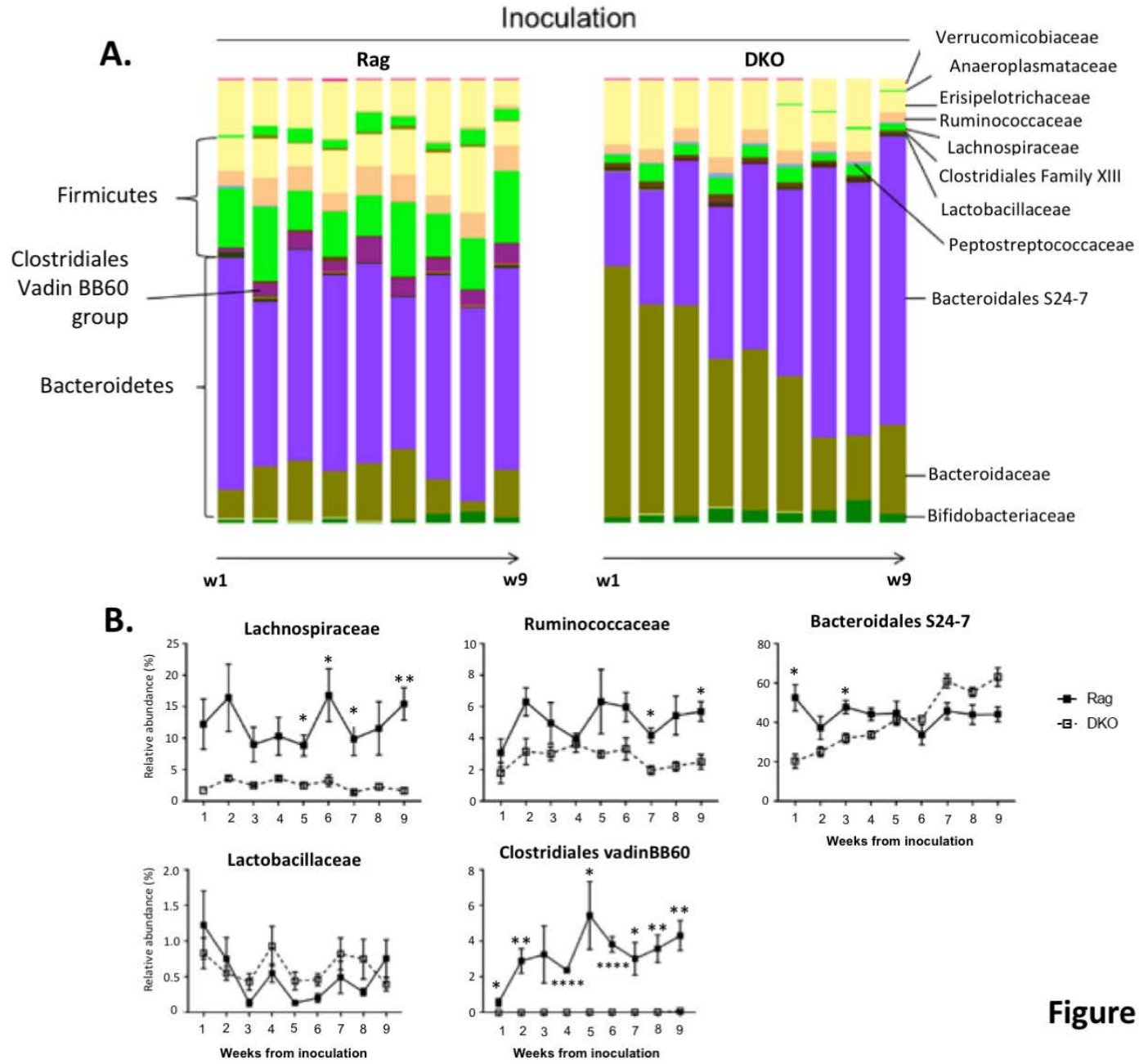
A.
Inoculation
Rag
DKO
Verrucomicobiaceae
Anaeroplasmataceae
Erisipelotrichaceae
Ruminococcaceae
Lachnospiraceae
Clostridiales Family XIII
Lactobacillaceae
Peptostreptococcaceae
Bacteroidales S24-7
Bacteroidaceae
Bifidobacteriaceae
Firmicutes
Clostridiales Vadin BB60 group
Bacteroidetes
w1
w9
w1
w9
B.
Lachnospiraceae
Ruminococcaceae
Bacteroidales S24-7
Lactobacillaceae
Clostridiales vadinBB60
Relative abundance (%)
Weeks from inoculation
Rag
DKO

Figure S4

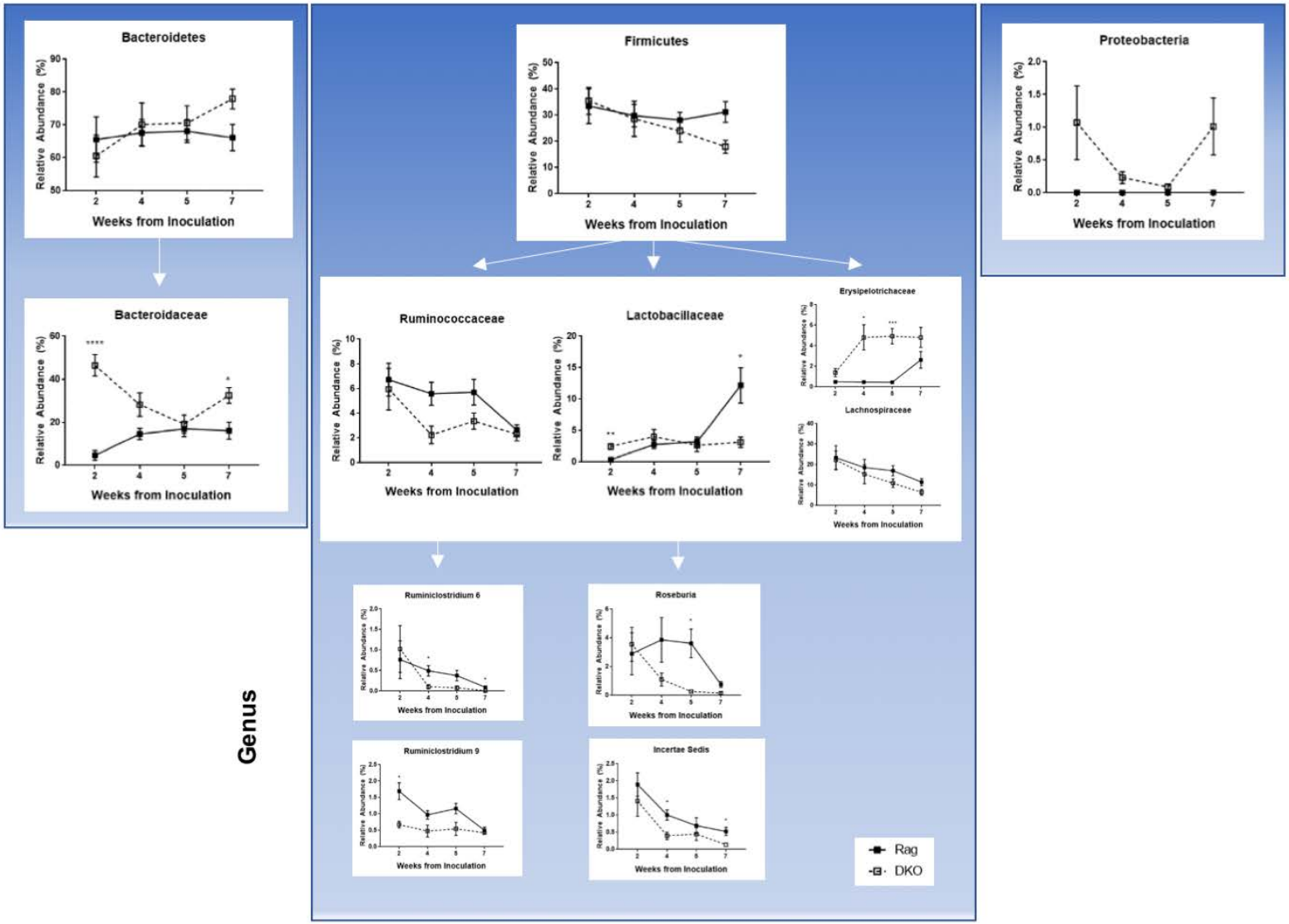
Phylum
Family
Genus
Bacteroidetes
Firmicutes
Proteobacteria
Bacteroidaceae
Ruminococcaceae
Lactobacillaceae
Erysipelotrichaceae
Lachnospiraceae
Ruminiclostridium 6
Roseburia
Ruminiclostridium 9
Incertae Sedis
Relative Abundance (%)
Weeks from Inoculation
Rag
DKO

Figure S5

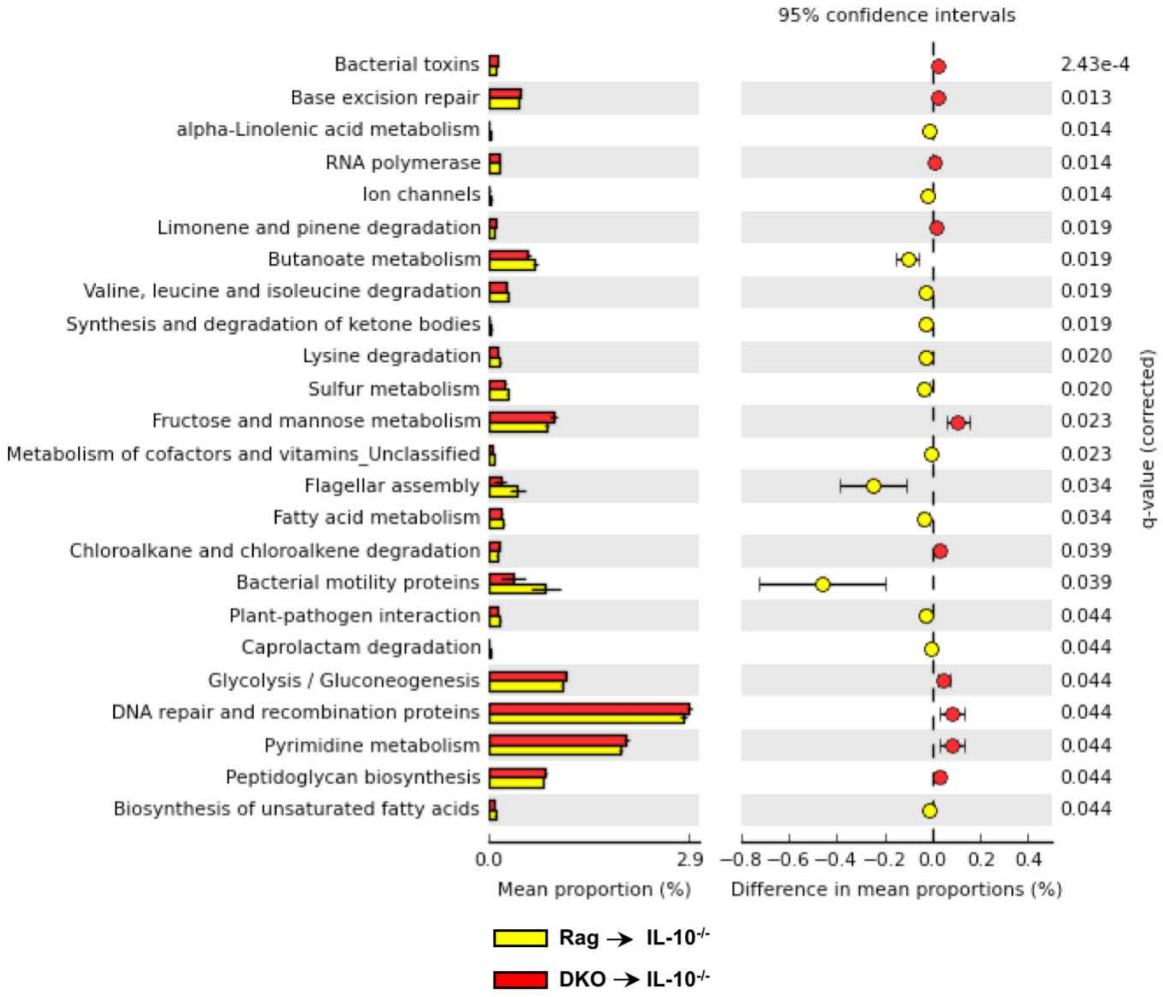
95% confidence intervals
Bacterial toxins
Base excision repair
alpha-Linolenic acid metabolism
RNA polymerase
Ion channels
Limonene and pinene degradation
Butanoate metabolism
Valine, leucine and isoleucine degradation
Synthesis and degradation of ketone bodies
Lysine degradation
Sulfur metabolism
Fructose and mannose metabolism
Metabolism of cofactors and vitamins_Unclassified
Flagellar assembly
Fatty acid metabolism
Chloroalkane and chloroalkene degradation
Bacterial motility proteins
Plant-pathogen interaction
Caprolactam degradation
Glycolysis / Gluconeogenesis
DNA repair and recombination proteins
Pyrimidine metabolism
Peptidoglycan biosynthesis
Biosynthesis of unsaturated fatty acids
2.43e-4
0.013
0.014
0.014
0.014
0.019
0.019
0.019
0.019
0.020
0.020
0.023
0.023
0.034
0.034
0.039
0.039
0.044
0.044
0.044
0.044
0.044
0.044
q-value (corrected)
0.0
2.9
Mean proportion (%)
−0.8 −0.6 −0.4 −0.2 0.0 0.2 0.4
Difference in mean proportions (%)
Rag → IL-10-/-
DKO → IL-10-/-

Figure S6